

THE KITT PEAK GALAXY REDSHIFT SURVEY WITH MULTICOLOR PHOTOMETRY: BASIC DATA

JEFFREY A. MUNN¹

Yerkes Observatory, University of Chicago, P.O. Box 258, Williams Bay, WI 53191-0258

DAVID C. KOO¹

University of California Observatories/Lick Observatory, Board of Studies in Astronomy and Astrophysics,
University of California, Santa Cruz, CA 95064

RICHARD G. KRON¹

Fermi National Accelerator Laboratory, MS 127, Box 500, Batavia, IL 60510

STEVEN R. MAJEWSKI^{1,2}

Department of Astronomy, University of Virginia, P.O. Box 3818, Charlottesville, VA 22903-0818; Observatories of the
Carnegie Institution of Washington, 813 Santa Barbara Street, Pasadena, CA 91101; and Yerkes Observatory,
University of Chicago, P.O. Box 258, Williams Bay, WI 53191-0258

MATTHEW A. BERSHADY^{1,2}

Department of Astronomy and Astrophysics, Pennsylvania State University, University Park, PA 16802

AND

JOHN J. SMETANKA¹

Department of Astronomy and Astrophysics, University of Chicago, 5640 S. Ellis Avenue, Chicago, IL 60637

Received 1995 July 20; accepted 1996 September 3

ABSTRACT

Redshifts, four-band photometry ($UB_J R_F I_N$), and astrometry are presented for faint galaxies in four widely separated fields. We provide the necessary information to enable well-defined, statistically complete subsamples of faint galaxies to be constructed from the master catalog. The redshift survey is 86% and 71% complete to $R_F \leq 18.5$ and $R_F \leq 19$, respectively, yielding 328 galaxies with reliable redshifts to $R_F \leq 19$, with a median redshift of 0.142. Adding the galaxies from the fainter statistical sample yields a total of 583 reliable redshifts with a median redshift of 0.202. An additional 156 redshifts in the same fields, but not part of the samples defined here, are also given. Of the 739 galaxy redshifts presented, 212 are for galaxies with $R_F > 20$.

Subject headings: astrometry — cosmology: observations — galaxies: distances and redshifts —
galaxies: photometry — surveys

1. INTRODUCTION

The current generation of telescopes and instrumentation has enabled large samples of ordinary galaxies—that is, galaxies not selected for special properties—to be measured for redshift, where the typical redshift is sufficiently high that evolutionary and cosmological effects are expected to be apparent. This direct empirical probe of processes that affect galaxies at earlier epochs forms the basis for tests of evolutionary models. Similarly, the evolution of the clustering properties of galaxies can now be traced directly to significant look-back times and compared to models of structure formation.

Faint galaxy redshift surveys are tedious and require large amounts of telescope time because the photon flux from distant galaxies is low and the noise background from the night sky is high. Nevertheless, because of the importance of these data, the required investment has been made by a number of research groups (e.g., Broadhurst, Ellis, & Shanks 1988; Cowie, Songaila, & Hu 1991; Colless et al. 1990; Songaila et al. 1994; Glazebrook et al. 1995; Lilly et al. 1995), and indeed faint galaxy redshift surveys are commonly featured in the scientific case for new optical tele-

scopes and instrumentation. Subsequent work in this field will extend the limits in apparent flux, explore large-scale structure with independent and larger samples, experiment with different selection algorithms, and take advantage of higher angular and spectral resolution.

In this paper, we present the results of a long-term redshift survey undertaken at Kitt Peak National Observatory with the Mayall 4 m telescope. These results are in the form of a catalog of the data: the photometry and astrometry, the redshifts and reliability of the redshifts, and information about the sample selection to enable the underlying statistical distribution functions to be recovered. A number of results and analyses previously undertaken on subsets of the survey (most recently by Bershaday et al. 1994, hereafter Paper III; Smetanka 1997) are based on the data presented in this paper.

It is worth recounting the original motivation for this redshift survey, because the galaxy selection and observing strategy reflect it. The cryogenic camera on the Mayall Telescope was the first publicly available instrument capable of multiple-object faint spectroscopy. As such, it enabled a direct check on the predicted field galaxy redshift distribution that had been derived from photometric information available at the time, namely, the single-color distribution of Kron (see Bruzual & Kron 1980; Tinsley 1980), extended by Koo (1981) to the four bands (three colors) of the present catalog. More specifically, Bruzual's models for evolving spectral energy distributions accounted for the dis-

¹ Visiting Astronomer, Kitt Peak National Observatory, National Optical Astronomy Observatories, which is operated by the Association of Universities for Research in Astronomy, Inc. (AURA), under cooperative agreement with the National Science Foundation.

² Hubble Fellow.

tribution of observed colors and the galaxy counts, where the key adjustable parameter was the form of the history of star formation in galaxies. The predicted shape of the redshift distribution was found to be sensitive to the particular formulation of the star formation history; thus the observed redshift distribution was expected to provide an excellent test of evolutionary models.

At the same time, it was recognized that the shape of the redshift distribution for a flux-limited sample could be used as a cosmological test: a higher q_0 model yields a higher median redshift and a more extended tail to high redshifts. Assuming that no systematic errors are introduced, the accuracy derivable from “photometric redshifts” (Baum 1962) is potentially sufficient for this purpose (Koo 1985), but of course, photometric redshifts require a calibration with respect to known, spectroscopic redshifts. Thus one of the original hopes was that our expected sample of a few hundred faint galaxies with redshifts would provide such leverage on determining the cosmological deceleration parameter q_0 , either directly or indirectly via calibration of the broadband colors (as attempted, for example, by Loh & Spillar 1986).

Because neither the value of q_0 nor the form of the history of star formation in galaxies could be considered to be known, the overall strategy was to obtain as many empirical constraints as practical for a large, faint, representative sample of galaxies and then to attempt to fit all the data simultaneously with a model that included both evolutionary and cosmological effects. Specifically, the data to be obtained for this purpose were the magnitudes in four bands spanning the full accessible range of wavelength, an image-size parameter for each galaxy, and redshifts to a limit in apparent flux. All of these data were to be obtained for a statistically complete sample, to enable the number of galaxies within some bin of color, magnitude, or redshift to also be used as an observable.

At the time we started the project, there were no other redshift surveys of faint field galaxies, and few redshift surveys based on a uniformly calibrated flux limit at any magnitude (Kirshner, Oemler, & Schechter 1978; Kirshner et al. 1981). One effort by Turner (1980) at intermediate magnitudes ($B \simeq 20$) succeeded in establishing that the median redshift to that depth was close to the expected value.

We chose to select our fainter sample of galaxies in the red spectral range to match the instrumental response of the Cryogenic Camera. It was necessary to experiment with the magnitude limit since almost everything depended on the quality of the sky subtraction (some aspects of which could be addressed by the observing technique, described in § 3). Even in the best circumstances, the precision of the sky subtraction was limited by focus variations across the CCD (ameliorated later by the provision of a custom field-flattener) and by flexure in the spectrograph. The other ingredient in the choice of the flux limit was the surface density of galaxies on the sky. We determined that slitlets should be at least 10" long to enable a good measure of the sky on both sides of a target galaxy. In order to take advantage of the full area of the CCD, it is necessary to reach sufficiently faint magnitudes that there are enough target galaxies. The combination of the size of the field of view of the Cryogenic Camera and the minimum slit length was a fortuitously good match to the depth of our photometric catalogs.

After the first few observing runs, it was clear that the distribution of redshifts (obtained from measurements of line positions from crude analysis on the mountain) was far from smooth. Rather, it appeared that the galaxies in one of the “pencil beam” volumes favored a small set of particular values (“spikes”), with few galaxies in between. The width of the spikes was not detectably greater than the accuracy of the on-the-mountain redshifts (say, 1000 km s⁻¹). Strong modulation of this sort could not be due to instrumental or other artificial effects, and hence we presumed that it was due to large-scale structure (Koo & Kron 1987), perhaps related to features like the Bootes void (Kirshner et al. 1981). Whatever the detailed interpretation, it became clear that the original motivation—the determination of the overall, smoothed redshift distribution to constrain models for galaxy evolution and cosmology—would require many widely spaced pencil beams to average out the effects of the individual spikes. Alternatively, one could use the pencil-beam data to study large-scale structure itself and its evolution over a significant interval of cosmic time (Koo, Kron, & Szalay 1987). As a result, the project that began as a test case for “long-term scheduling” at Kitt Peak became even longer.

This paper presents the photometric and spectroscopic results of our faint galaxy redshift survey in four separate regions of the sky. The data are presented such that statistical analyses can be undertaken. As mentioned earlier, we have already derived several results based on these data; in this paper, the analysis is restricted to a few summary plots. In the context of the pursuit of the grand questions of the evolution and origin of galaxies, the cosmological model, and the development of large-scale structure, these data complement the other faint galaxy redshift surveys that have been undertaken in the meantime in terms of photometric information, sampling, completeness, and depth. To make substantial progress with respect to these surveys will require much larger telescopes, higher angular resolution, extended wavelength coverage, and, inevitably, continued major investment in observing time.

2. PHOTOMETRY

2.1. Observations

The $UB_J R_F I_N$ photographic survey of selected fields has been conducted with the prime-focus plate camera on the Mayall 4 m telescope at Kitt Peak National Observatory (KPNO) since 1974. The nature of the imaging survey is described by Kron (1980, hereafter Paper I) and Koo (1986, hereafter Paper II), including thorough discussions of the photometric properties of the plates and the effective passbands of the emulsion/filter/telescope combinations. Transformation equations between the $UB_J R_F I_N$ and $UBVRI$ photometric systems are given by Majewski (1992).

Table 1 lists the four fields: Selected Area 68, Lynx 2 (also known as Selected Area 28), Selected Area 57, and Herc 1. All four fields were selected based partly on their high Galactic latitude. Additionally, fields SA 57 and SA 68 were selected because they contain photoelectric stellar magnitude sequences to $B = 22.5$, while fields Herc 1 and Lynx 2 were selected to be approximately evenly spaced in right ascension from the first two fields. The plates used to create the astrometric and photometric catalogs in SA 57 and SA 68 are listed in Paper I and Paper II. The plates used in Herc 1 are listed in Paper III. Table 2 lists the plates used in

TABLE 1
FIELDS

Name (1)	α_{1950} (2)	δ_{1950} (3)	Area (4)	l (5)	b (6)
SA 68	00 14 53	+15 36 48	0.214	111.0905	-46.1982
Lynx 2	08 41 43.7	+44 46 42	0.384	176.0245	+38.4462
SA 57	13 06 15	+29 39 06	0.284	63.1501	+85.6599
Herc 1	17 18 57.6	+49 58 22	0.384	76.6363	+34.8198

Col. (1).—Field name.

Col. (2).—Right ascension in hours, minutes, and seconds of catalog center (1950 equinox).

Col. (3).—Declination in degrees, arcminutes, and arcseconds of catalog center (1950 equinox).

Col. (4).—Area covered by the catalog in square degrees. The SA 57 and SA 68 catalogs cover circular fields, 37'3 and 31'9 in diameter, respectively, with some bad scan lines and areas around bright stars excluded. The Lynx 2 and Herc 1 catalogs cover square fields, each 37'18 on a side.

Cols. (5), (6).—Galactic longitude and latitude in degrees of catalog center.

Lynx 2. The field of the camera is 50' in diameter, but in practice the cataloged objects cover a smaller area (Table 1).

2.2. Reductions

The photometric reductions for SA 57 and SA 68 are described in previous papers (Paper I; Paper II) and will not be further discussed here, except for new saturation and photometric zero-point corrections described later. The reductions for Herc 1 and Lynx 2 employed different methods, which are detailed below.

Each photographic plate for Herc 1 and Lynx 2 was scanned on the Midwest Astronomical Data Reduction and Analysis Facility's PDS microdensitometer. The scanning was performed in 20 μm steps, using a 20 μm^2 beam and a 50 μm^2 photomultiplier entrance aperture. Because of hardware limitations, only one-quarter of a plate could be scanned at once; we selected an overlap of 99 rows and 99 columns between each plate quadrant. The scanned quadrants were reassembled into a single image, using the overlap regions to account for slow changes in the gain (typically 1% over the four scans required to complete one plate). Plate densities were transformed to relative intensities by fitting a sixth-order polynomial to the set of 16 calibration spots of known relative intensities imprinted on each plate during its exposure.

The detection, classification, and measurement of instrumental parameters of objects were performed separately for each plate by using the Faint Object Classification and Analysis System (FOCAS, version 3.3). The process is briefly summarized here, primarily to note the various

options and parameters that were used in the otherwise largely automated reductions, as well as to note where human intervention was necessary. A detailed discussion of FOCAS and its algorithms is given by Jarvis & Tyson (1981) and Valdes (1982).

Object detection was performed on the raw scanned images (i.e., with pixels measuring plate densities), convolved with the default detection filter in FOCAS. Any contiguous set of 15 or more pixels (including diagonals) in which the value of each pixel exceeded the sky value by at least 2.5 times the square root of the sky variance was considered a detected object. For each object, instrumental parameters were measured using the unconvolved image (i.e., not convolved with the detection filter), with pixel values transformed to relative intensities. A local sky value was determined from the mode of the Gaussian-convolved histogram of the pixel values contained within a rectangular "window frame" 6 pixels wide surrounding a 10 pixel-wide rectangular "window frame" whose inner border circumscribes the object's detection isophote. Merged objects were split into separate objects, using the default FOCAS parameters. Large galaxies tended to be split into many individual detections. These were examined directly (by displaying their scanned images on a computer screen) and, when appropriate, fixed to be a single detection (with an isophote encompassing the spurious daughter objects) in the catalog. An empirical point-spread function was then constructed by summing the brightest 20 unsaturated stars whose first moments fell within a specified range. This was then used with a custom set of classification rules to classify each object.

The FOCAS reductions yielded a separate catalog of objects for each plate, thus giving seven catalogs in each of the two fields. The quality of the individual catalogs was checked by comparing the objects detected on different plates within a field. All bright objects that were missing from one or more plates, that were classified differently on different plates, or that had unusual classifications (i.e., anything other than the FOCAS classifications "star," "galaxy," or "fuzzy star") were checked by eye. Obvious false detections and other artifacts were removed from the catalogs, and objects with differing classifications were assigned a final classification by inspection. These checks were performed to the following magnitude limits: in Herc 1, $U < 22$, $B_J < 22$, $R_F < 21$, $I_N < 19.5$; in Lynx 2, $U < 21$, $B_J < 22$, $R_F < 21$, $I_N < 20$. Nearly all the galaxies with reliable redshifts presented here are brighter than these limits. A study of the galaxy counts as a function of magnitude shows that the photometric catalogs are complete to at least

TABLE 2
LYNX 2 CATALOG PLATE SET

Plate (MPF)	Band	Date (UT)	Exposure (minutes)	Corrector	Emulsion	Filter	UT (start)	h.a. (end)	r_1^a (arcsec)
3619	U	1982 Jan 31	150	UBK-7	IIIa-J	UG5	0625	1W26	0.76
1288	B_J	1974 Oct 19	45	UBK-7	IIIa-J	GG385	0943	3E51	0.93
1289	B_J	1974 Oct 19	45	UBK-7	IIIa-J	GG385	1030	3E03	0.91
1298	R_F	1974 Oct 20	65	BK-7	127-02 ^b	GG495	0957	3E13	0.76
1299	R_F	1974 Oct 20	67	BK-7	127-02	GG495	1105	2E04	0.70
3626	I_N	1982 Feb 1	45	UBK-7	IV-N	RG695	0348	2E53	1.20
3627	I_N	1982 Feb 1	60	UBK-7	IV-N	RG695	0439	1E47	1.22

^a Intensity-weighted first radial moment of the average stellar profile for unsaturated stars.

^b Emulsion 127-02 is a predecessor of IIIa-F.

a magnitude fainter than these limits, and well past the limits of the spectroscopic sample.

The photometry of some of the brighter galaxies is affected by plate saturation in their high surface brightness cores. Paper III develops a technique to correct this effect and applies the technique to the fields SA 57, SA 68, and Herc 1. The photometry presented here includes correction for saturation effects in all those fields, but it has not yet been applied to the Lynx 2 photometry. Based on the other three fields, we expect only a couple of the brightest objects in Lynx 2 to be seriously affected (corrections of greater than 0.1 mag), with perhaps another half-dozen affected at the level of 5%–10%.

Photometric zero points were derived from *UBVRI* CCD photometry by Majewski et al. (1994) for $UB_J R_F I_N$ in SA 57 and Herc 1, and by Majewski et al. (1997) for $UB_J R_F I_N$ in Lynx 2 and R_F and I_N only in SA 68. In SA 68, the B_J zero point is taken from Paper I, and the U zero point is determined by forcing the stellar locus for unsaturated stars in the $U - B_J$, $B_J - R_F$ color-color diagram to match the stellar loci in the other three fields. The 1σ errors in magnitudes for the $UB_J R_F I_N$ zero points are 0.071, 0.021, 0.105, and 0.160 in SA 57; 0.05, 0.03, 0.023, and 0.017 in SA 68; 0.047, 0.122, 0.059, and 0.065 in Herc 1; and 0.106, 0.065, 0.061, and 0.039 in Lynx 2.

3. SPECTROSCOPY

Just as the photographic plate survey supports many ongoing programs, the field galaxy spectroscopy reported here is but one of a number of different spectroscopic surveys based within the same photographic fields. Spectroscopic observing runs often targeted objects from multiple programs. As such, this paper describes the details of the observations and data reduction procedures for all of the spectroscopic observing runs within the various spectroscopic surveys. Additional papers concerning this or other spectroscopic surveys supported by the various observing runs will reference this paper for a description of the observations and data reductions.

3.1. Observations

The spectroscopic observations were obtained with the KPNO Mayall 4 m telescope. The earliest observations (1981–1987) were conducted with the Cryogenic Camera, a low-resolution CCD spectrometer that, in place of the normal spectrograph slit, accepts aperture plates with a 5' diameter field of view. A standard set of plates is available, offering single slits of differing widths and lengths. Both 2".5 and 3".2 wide slits were used in this mode. Multiaperture capabilities were first provided by multihole aperture plates (Butcher 1982). Each aluminum plate is drilled with 20–40 holes (2".5 diameter) at the focal-plane positions of the targets. We used a beam-switching technique whereby each plate was drilled such that half the holes targeted objects for one telescope pointing while the remaining holes targeted objects for a second telescope pointing, offset typically by 7' from the first pointing. Multiple exposures were then taken, alternating between the two telescope pointings, so that a given hole alternates between object and sky on different exposures.

For the 1982 October and 1983 March runs, we attempted to improve the sky subtraction by replacing the holes with 2".5 wide by 15" long slitlets. The multislit masks were designed by hand, and blank aluminum plates provided by

KPNO were drilled at the University of Chicago. The attempt proved successful, and KPNO subsequently modified their software and drilling procedures to support multislit masks. They later further modified their procedures to allow the individual slitlets to extend out in length as far as possible without interfering with the light from another slitlet. In 1985, KPNO replaced the aluminum plates with high-contrast photographic film, offering the same multislit capabilities at considerable cost savings, but with a 10% light loss due to the film base. For all Cryogenic Camera observations, a quartz-dome flat exposure and a helium-neon-argon lamp wavelength calibration exposure were obtained each time the aperture plate was moved in or out of position.

From 1988 to 1991, observations were conducted using Nessie (Barden & Massey 1988), a plugboard fiber-optic feed assembly with 47 fibers (2".1 diameter) over a 40' field of view, coupled to the Ritchey-Chrétien spectrograph. Since 1992, Hydra has been used, a robotic fiber-optic feed assembly with 97 fibers (2" diameter) over a 40' field of view, coupled to the bench spectrograph (Barden et al. 1993). Five to 10 sky fibers were used for each Nessie and Hydra configuration, with no beam-switching. Quartz-dome flat frames were obtained for each new fiber configuration. For both Nessie and Hydra, the spectrograph is located off the telescope, and thus flexure is absent. Wavelength calibration exposures, using a helium-neon-argon lamp, were therefore taken once at the beginning of each night, as well as occasionally at the end of the night to check the stability. Table 3 lists the spectroscopic observing runs, and Table 4 gives the various spectral ranges, spectral resolutions, and other details of the instrumental configurations.

3.2. Data Reductions

The data were reduced using various versions of the Image Reduction and Analysis Facility (IRAF).³ The APEXTRACT package (Valdes 1986) was used for long-slit, multislit, and multihole reductions, and the NESSIE and HYDRA packages were used for the multifiber data. Standard reduction procedures based on these packages were followed, so a detailed description of the reductions will not be given, but a few key parameters and decisions will be noted. Optimal extraction was not used. A second-order polynomial was used to fit the sky in the multislit and long-slit data. A polynomial (seventh order for the Cryogenic Camera data, third order for the Nessie and Hydra data) was fitted to the helium-neon-argon lines to determine the wavelength calibration, yielding rms residuals of roughly 0.3 pixels for Cryogenic Camera spectra and 0.1 pixels for Nessie and Hydra spectra. Flexure during the Cryogenic Camera exposures, analyzed using night-sky lines, was found to be less than 0.1 pixels, and thus no corrections were made for it. No flexure was detected during the course of an evening with Nessie and Hydra, as expected with a bench-mounted spectrograph.

Redshifts were determined by cross-correlation with a template spectrum of the core of M31 (kindly provided by H. Spinrad) for absorption-line spectra and with Gaussian fits to individual emission lines in emission-line spectra.

³ IRAF is distributed by the National Optical Astronomy Observatories, which is operated by the Association of Universities for Research in Astronomy, Inc. (AURA), under cooperative agreement with the National Science Foundation.

TABLE 3
OBSERVING RUNS

Code (1)	UT Dates (2)	Useful Percentage (3)	Setup (4)	Apertures (5)	Fields (6)
a	1981 Oct 3–7	100	I	h, l	1
b	1982 Jun 15–22	60	I	h, l	2, 3
c	1982 Oct 9–13	70	I	h, l, m	1
d	1983 Mar 16–21	50	I	l, m	2, 4
e	1983 Sep 28–Oct3	0	I	l, m	1
f	1984 Mar 4–8	80	II	l, m	2, 3, 4
g	1984 Nov 21–25	10	II	l, m	1
h	1985 Feb 17–19	40	II	l, m	4
i	1985 Apr 20–23	60	II	l, m	2, 3
j	1985 Sep 13–16	60	II	l, m	1, 3
k	1986 Feb 4–6	60	III	l, m	2, 4
l	1986 May 14–17	80	II	l, m	2, 3
m	1987 Apr 4–6	50	II	l, m	3, 4
n	1987 Dec 16–19	0	II	l, m	1
o	1988 Jun 15–17	25	II	n	2, 3
p	1988 Jul 5–7	0	II	n	2, 3
q	1989 Jan 6–9	10	II	n	1, 2, 4
r	1989 May 30–Jun 2	100	II	n	3
s	1989 Jul 1–5	75	II	n	1, 3
t	1989 Sep 26–29	65	II	n	1, 3, 4
u	1990 Oct 20–23	60	IV	n	1, 4
v	1991 Jan 18–22	35	V	n	1, 2, 4
w	1991 Mar 18–20	10	VI	n	2, 4
x	1991 May 12–15	70	VII	n	3
y	1991 Sep 11–13	60	VIII	n	1, 3
z	1992 Oct 21–24	100	IX	f	1, 4

Col. (1).—Code by which each run is referenced throughout this paper.

Col. (2).—UT dates of the observing run.

Col. (3).—Percentage of observing time during which atmospheric conditions were sufficiently good to allow execution of the primary observing program.

Col. (4).—Instrumental setup used. Cross-reference to col. (1) in Table 4.

Col. (5).—Aperture mask types used: (h) multiholes; (l) long slit; (m) multislits; (n) Nessie multifibers; (f) Hydra multifibers.

Col. (6).—Fields observed. (1) SA 68; (2) SA 57; (3) Herc 1; (4) Lynx 2.

Cross-correlations followed the prescription of Tonry & Davis (1979), using software written by us as well as the RV package of IRAF. Emission lines, cosmic rays, poorly subtracted night-sky lines, and other glitches in the spectra were linearly interpolated over before cross-correlation.

Each spectrum and cross-correlation was inspected by eye. Estimating the errors in a cross-correlation redshift is difficult at best, and a detailed error estimate for each redshift measurement was not attempted. A general error analysis leads to a conservative error estimate for typical acceptable redshifts of $\sim 250 \text{ km s}^{-1}$. Accordingly, heliocentric corrections have not been applied.

4. THE SURVEY

The primary goal of the field galaxy spectroscopic survey is to obtain reliable redshifts for galaxies in two separate samples: a bright sample, complete for all galaxies with $R_F \leq 19$ or $B_J \leq 20$ over the entire field of view of each of the four photometric fields; and a faint sample, statistically complete to fainter magnitude limits in R_F . The basic observing strategy (adopted in 1981, when the Cryogenic Camera was the only spectrometer on the 4 m telescope offering multiobject capabilities) was to obtain spectra for the bright sample one at a time with single short (5–30 minute) exposures, using long slits during poor weather, and to obtain spectra for the faint sample many at a time using the multihole and multislit masks, with long (1–4 hr) total integration times, split up into 15–30 minute exposures. The mask positions were often chosen to include faint objects from some of the other programs, most notably the QSO candidate and radio source surveys. Thus the selection function for the faint sample is largely determined by the target selection used when creating the multiaperture masks. A complete description of this process follows.

4.1. Target Selection

Each multiaperture mask covers a circular field approximately $5'$ in diameter, in contrast to the approximately $40'$ diameter fields of the photometric catalogs. Ideally, the positions of each mask should be chosen at random within each $40'$ field. In practice, the following constraints were put on the mask centers: First, the mask centers were often chosen so that the mask would include certain special targets—usually objects that are part of other programs—including galaxies in the bright galaxy sample, QSO candidates, known radio sources, UV-excess galaxies, members of galaxy clusters, subdwarf stars, and M dwarf stars.

TABLE 4
INSTRUMENTAL CONFIGURATIONS

Code (1)	Spectrograph (2)	Detector (3)	Grating/Grism (4)	Lines (5)	Order (6)	Range (7)	Dispersion (8)	Resolution (9)
I	Cryocam	Cryocam	770	300	1	4550–7850	4.16	15
II	Cryocam	Cryocam	770	300	1	4500–7900	4.31	15
III	Cryocam	Cryocam	810	150	1	4500–9700	9.68	30
IV	RC	TE1K	KPC-10A	316	1	4400–7200	2.77	8
V	RC	TI2	B&L 250	158	1	3545–6215	3.44	15
VI	RC	TE1K	B&L 250	158	1	3695–9265	5.45	15
VII	RC	TE1K	KPC-10A	316	1	4945–7775	2.77	8
VIII	RC	TE1K	KPC-10A	316	1	3900–6700	2.77	8
IX	Bench	T2KB	KPC-10A	316	1	3900–7800	2.00	8

Col. (1).—Code by which each instrumental configuration is referenced in col. (4) of Table 3.

Col. (2).—Spectrograph used.

Col. (3).—Detector used.

Col. (4).—Grating or grism used.

Col. (5).—Lines per millimeter for the grating or grism.

Col. (6).—Spectrographic order used.

Col. (7).—Wavelength coverage. For multihole and multislit aperture masks, the central wavelength for individual spectra may be shifted redward or blueward from the nominal value by up to 25% of the spectral coverage.

Col. (8).—Spectral dispersion in angstroms per pixel.

Col. (9).—Spectral resolution (FWHM) in angstroms.

Indeed, centers were frequently chosen primarily to maximize the number of such special targets that could be observed. Second, masks were frequently positioned to reobserve targets from previous masks for which a reliable redshift had not been obtained. Third, a star with a magnitude $R_F < 18$ was usually included within the mask to adjust the pointing of the telescope before the beginning of the exposure. Fourth, in the case of the multihole masks, the two offset positions were constrained to be separated by approximately $7'$.

Once a mask center was determined and the special targets selected, all galaxies within the circular field of view of the mask ($165''0$ radius for all multihole masks and the hand-designed multislit masks from the 1992 October and 1993 March runs; $156''3$ radius for all other multislit masks) and brighter than some magnitude limit in R_F were selected from the catalog as potential mask targets (for multihole masks in SA 57 and SA 68 created for the 1981 October and 1982 June runs, fainter galaxies were selected within smaller radii from the mask centers: $r < 149''$ for $21 \leq R_F < 22$; $r < 106''$ for $22 \leq R_F < 22.5$). These were added to the list of special targets, and a weight was assigned to each object in the final list of candidate targets. A typical set of weights is 1000 for special targets, 500 for galaxies with $R_F < 21$, 100 for $21 \leq R_F < 22$, and 10 for $22 \leq R_F < 22.5$. This list of candidate targets and weights was fed to a KPNO program, which selected a final list of targets from the list of candidates and determined the physical positions of the apertures (and lengths for slitlets), to maximize the summed weight for the selected set of final targets while assuring that spectra from the chosen targets do not overlap. The position angle of the spectrograph is allowed to vary in this optimization. Occasionally, after an initial run of the target selection program, individual weights or positions were adjusted and the program rerun to ensure that specific targets were selected.

Table 5 lists all multiaperture masks used in the course of the various spectroscopic surveys. For the purpose of defining the faint field galaxy sample, the important information to note for each mask is the list of special targets (col. [9]), each of which is identified, as well as the reason for its selection as a special target. Redshifts are given in Table 5 for all special targets that were morphologically classified as stellar (including QSO candidates), and which therefore are not part of the catalogs of extended objects presented in Table 6. The redshifts of the remaining special targets may be found in Table 6.

4.2. Catalogs

Table 6 presents the astrometry, photometry, and redshifts for all objects morphologically classified as galaxies, and which have been observed spectroscopically and/or belong in the bright R_F or B_J samples ($R_F \leq 19$ or $B_J \leq 20$). Objects are listed in order of increasing R_F magnitude within each of the four fields. Each redshift is assigned a quality factor, ranging from 0 to 6, assigned as follows: Each spectrum was inspected by at least two of the authors working together, who counted the number of definite and probable features, where a feature may be either an absorption or emission line, or a continuum feature, such as the 4000 \AA or G -band breaks. The overall quality, q , was then assigned according to the formula

$$q = \min [6, \min (1, N_{\text{def}}) + 2N_{\text{def}} + N_{\text{prob}}],$$

where N_{def} and N_{prob} are the number of definite and probable features, respectively. This is admittedly a subjective process, but we estimate a definite feature to have less than a 5% chance of being spurious and a probable feature less than 50%. For most purposes, we adopt $q > 2$ as the requirement for a reliable redshift, meaning at least one definite or three probable features, which means a $\geq 95\%$ to $(1 - 0.5^3)$ or $\geq 87\%$ reliability, respectively. In all cases in which one definite and no other probable features were found, the one definite feature is a strong emission line that has been identified as $\text{O II } \lambda 3727$. Objects lacking a redshift quality rating were not observed spectroscopically. A value of $q = 0$ means that the object was selected for the redshift survey and was included in a mask that yielded useful data, but the spectrum was too poor to yield identifications of any features. Objects with $z = 0$ were inspected by eye on one or more photographic plates; all were found to be stars whose morphological classification was confused by blending with an adjacent extended object. Missing colors are due to the failure to detect the object in one or more photometric bands, as a result of either the intrinsic faintness of the object, blending with adjacent objects, or plate glitches. The magnitudes and colors presented are averaged for those objects detected on two separate plates in the same passband. The astrometry is derived from the single plate in each field judged to provide the best astrometry. The random errors in the astrometry are approximately $0''.3$ in SA 57, SA 68, and Lynx 2 and $0''.45$ in Herc 1.

The apertures in which the magnitudes and colors were measured differ between fields SA 57 and SA 68 and fields Herc 1 and Lynx 2. In SA 57 and SA 68, for each object, the radial flux profiles on the two B_J and two R_F plates were summed and the first intensity-weighted radial moment, r_1 , of this summed profile determined. Magnitudes were then measured on each plate within a circular aperture of radius $2r_1$. The same aperture was used for each object on all plates. Both the R_F magnitude and colors derive from this $2r_1$ photometry. In Herc 1 and Lynx 2, because the FOCAS reductions were conducted on each plate independently, isophotal and total magnitudes were measured within different apertures on each plate. To avoid the effects that passband-dependent apertures may have on the integrated colors, the tabulated colors were measured within fixed $2''$ radius circular apertures. The R_F magnitude is the FOCAS total magnitude (the flux contained in an area determined by growing the detection isophote until the enclosed area exceeds twice the original enclosed area). The rationale for and implications of these choices for the integrated photometry are discussed in detail in Paper III.

The random photometric errors at faint magnitudes are dominated by the sky noise in the measuring aperture. Since the quantity $2r_1$ for faint objects does not vary over a wide range, the error in flux for faint objects in SA 57 and SA 68 is roughly constant, independent of the object's magnitude (Paper I). This approximation is even more valid for the constant $2''$ radius aperture photometry for fields Herc 1 and Lynx 2. Thus the random errors in magnitude are expected to scale with magnitude as

$$-2.5 \log (1 \pm \sigma 10^{0.4(m - m_0)}),$$

where σ is the random error expressed as the fraction of the flux at a reference magnitude m_0 . Values for σ and m_0 for each band in each field are tabulated in Table 7. Note that in fields Herc 1 and Lynx 2 this yields the random errors for

the 2" radius aperture magnitudes used in the derivation of the colors. The random error in the R_F magnitude, where FOCAS total magnitudes are quoted, will be larger.

4.3. Bright Sample

Figures 1 and 2 show the completeness of the redshift survey in each of the four fields separately as a function of

magnitude for the R_F -limited ($R_F \leq 19$) and B_J -limited ($B_J \leq 20$) bright samples. The lower completion rates in Herc 1 and Lynx 2 reflect their more recent addition to the bright spectroscopic survey. The B_J -limited samples in SA 57 and SA 68 are 96% and 97% complete ($q > 2$), respectively, to $B_J \leq 20$. SA 68 is 91% complete in the R_F -limited sample to $R_F \leq 19$ while SA 57 is only 82% complete. More

TABLE 5
MULTIAPERTURE MASKS

Sequence (1)	Type (2)	KPNO (3)	ID (4)	α_{1950} (5)	δ_{1950} (6)	Runs (7)	T (8)	Special Targets (9)
A. SA 57 Multiaperture Masks								
A	Holes	223	2AC-A	13 07 16.50	29 39 52.0	b	4000	Radio source: 11824
B	Holes	223	2AC-C	13 06 53.20	29 43 42.0	b	4000	QSO candidates: 12536 ($z = 0.420$, $q = 6$), 13412 ($z = 2.082$, $q = 5$), 13786 (star, $q = 4$)
C	Holes	240	3AB-A	13 06 40.20	29 32 54.0	b	4000	QSO candidates: 5422 ($z = 1.083$, $q = 4$), 5482 ($z = 0.4534$, $q = 6$), 6442 ($z = 2.124$, $q = 5$), 7031 (star, $q = 4$)
D	Holes	240	3AB-B	13 07 00.20	29 29 24.0	b	4000	QSO candidates: 2888 ($z = 1.334$, $q = 6$), 3707 ($q = 0$), 4855 ($z = 1.305$, $q = 3$), 5003 (star, $q = 3$)
E	Holes	241	3AC-A	13 06 42.70	29 33 29.0	b	2000	Retarget C
F	Holes	241	3AC-C	13 06 03.70	29 36 29.0	b	4000	QSO candidates: 7567 ($z = 1.812$, $q = 5$), 7624 ($z = 1.738$, $q = 4$), 8945 ($z = 0.608$, $q = 3$), 9361 ($q = 0$), 9877 ($z = 2.120$, $q = 5$)
G	Holes	242	4AB-A	13 05 28.00	29 39 45.0	b	4000	II Zw 1305.4+2941 galaxy cluster QSO candidate: 11334 ($q = 0$)
H	Holes	242	4AB-B	13 05 51.00	29 39 45.0	b	4000	QSO candidates: 9877 ($z = 2.120$, $q = 5$), 9934 ($z = 2.530$, $q = 5$), 9980 ($z = 1.545$, $q = 4$), 10405 ($q = 0$)
I	Holes	244	5AC-A	13 05 36.00	29 30 45.0	b	4000	Chosen to be far away from A and M to maximize angular coverage
J	Holes	244	5AC-C	13 05 39.50	29 23 45.0	b	4000	QSO candidates: 352 (star, $q = 2$), 441 ($z = 0.652$, $q = 3$), 1215 (star, $q = 6$), 1501 ($z = 0.499$, $q = 6$)
K	Holes	245	5AD-A	13 05 37.00	29 30 50.0	b	4000	Retarget I
L	Holes	245	5AD-D	13 05 11.00	29 34 30.0	b	4000	QSO candidates: 7042 ($z = 0.525$, $q = 6$), 7701 ($q = 0$), 7822 ($z = 2.458$, $q = 5$)
M	Slits	...	M1A2	13 05 38.00	29 51 00.0	d	4000	Galaxy cluster 1305 at $z = 0.95$: 18532, 18593, 18737, 18793. QSO candidates: 17750 ($z = 1.179$, $q = 6$), 16713 ($z = 0.993$, $q = 4$)
N	Slits	...	M1A3	13 05 38.00	29 52 06.3	(d), f	16000	Retarget M
O	Slits	...	M2C2	13 06 52.76	29 44 00.0	d	4000	Retarget B
P	Slits	...	M3A2	13 06 41.46	29 33 33.1	d, f	10000	Retarget C
Q	Slits	...	M3B2	13 07 06.20	29 29 25.0	d	6000	Retarget D. QSO candidate: 3977 ($q = 0$)
R	Slits	...	M5A2	13 05 35.52	29 31 00.0	d	8000	Retarget I
S	Slits	...	M5A3	13 05 34.00	29 31 00.0	(d), f	12000	Retarget I
T	Slits	39	M1A4	13 05 42.00	29 52 00.0	f	9500	Retarget M
U	Slits	40	M1B2	13 05 57.00	29 48 00.0	f, i	7000	QSO candidate: 15180 ($z = 1.797$, $q = 5$)
V	Slits	41	M1C2	13 06 20.20	29 52 25.0	(f), i	4000	QSO candidates: 19387 ($z = 1.461$, $q = 4$), 18607 ($q = 0$), 18414 ($q = 1$)
W	Slits	42	M4B2	13 05 55.70	29 40 30.0	f	3000	Retarget H
X	Slits	43	M5AJ	13 05 40.80	29 31 20.0	f	11800	Retarget I. Faint B_J galaxies: 4998, 5769, 5826, 5590, 5921, 5448, 5946, 4972, 5473, 5636
Y	Slits	44	M5D2	13 05 08.39	29 35 30.0	f	2500	Retarget L
Z	Slits	185	M1A5	13 05 35.73	29 52 00.0	i	9000	Retarget M
AA	Slits	186	M2A4	13 07 16.30	29 40 20.0	i	4500	Retarget A
BB	Slits	189	N13429	13 05 00.47	29 43 25.4	i	3000	Bright galaxy: 13429
CC	Slits	190	N17604	13 07 04.30	29 50 55.0	i	2000	Bright galaxy: 17604
DD	Slits	191	N1564	13 05 35.01	29 25 40.0	i	3000	Bright galaxy: 1564. Partially retarget J
EE	Slits	192	N2097	13 06 28.87	29 26 45.0	i	2000	Bright galaxy: 2097
FF	Slits	193	N1392	13 06 10.00	29 25 40.0	i	3000	Bright galaxy: 1665. QSO candidate: 1392 ($z = 3.077$, $q = 6$)
GG	Slits	253	M601	13 06 47.50	29 51 00.0	l	4000	QSO candidates: 18122 ($z = 2.025$, $q = 3$), 18996 (star, $q = 4$). Bright galaxy: 16599
HH	Slits	255	M603	13 04 58.50	29 40 00.0	l	4000	QSO candidates: 10028 ($z = 0.646$, $q = 3$), 12259 ($q = 1$), 11255 ($q = 0$). Bright galaxies: 11827, 10630
II	Slits	256	M604	13 05 17.00	29 49 40.0	l	4000	QSO candidates: 16713 ($z = 0.993$, $q = 4$), 18170 ($z = 0.586$, $q = 3$), 17671 ($z = 0.518$, $q = 3$)
JJ	Slits	258	M606	13 06 17.00	29 40 00.0	l	4000	QSO candidates: 10601 ($z = 0.438$, $q = 6$), 11604 ($q = 0$), 11450 ($z = 0.959$, $q = 3$), 9361 ($q = 0$)
KK	Slits	259	M607	13 06 24.01	29 52 00.0	l	4000	QSO candidates: 19387 ($z = 1.461$, $q = 4$), 18607 ($q = 0$), 17731 ($z = 0.663$, $q = 3$). Retarget V
LL	Slits	262	M610	13 07 17.00	29 36 40.0	l	3300	QSO candidates: 8956 ($z = 0.439$, $q = 3$), 7756 ($q = 0$), 8954 ($z = 0.319$, $q = 6$). Partially retarget A
MM	Slits	263	M611	13 05 43.00	29 33 00.0	l	4000	QSO candidates: 5643 ($z = 0.983$, $q = 3$), 7447 ($q = 0$), 4882 ($z = 1.468$, $q = 2$). Bright galaxy: 6689
NN	Slits	264	M612	13 06 11.50	29 45 36.0	l	5000	QSO candidates: 13966 ($z = 0.951$, $q = 3$), 15248 ($q = 1$), 15180 ($z = 1.797$, $q = 5$)
OO	Slits	268	M616	13 07 34.00	29 41 00.0	l	4000	QSO candidate: 10046 ($z = 2.876$, $q = 6$). Radio source: 52W047 (outside catalog, $q = 0$). Partially retarget A

TABLE 5—Continued

Sequence (1)	Type (2)	KPNO (3)	ID (4)	α_{1950} (5)	δ_{1950} (6)	Runs (7)	T (8)	Special Targets (9)
B. SA 68 Multiaperture Masks								
A	Holes	132	1AB-A	00 14 27.73	15 31 42.0	a	10000	QSO candidate: 5748 ($z = 1.908, q = 6$). Radio source: 5970 (stellar, $q = 0$)
B	Holes	132	1AB-B	00 14 27.73	15 24 42.0	a	18000	Radio sources: 1557, 3414
C	Holes	133	2AB-A	00 14 28.97	15 51 14.0	a	15000	QSO candidates: 17190 ($z = 1.169, q = 4$), 17169 ($z = 0.356, q = 6$). Radio source: 16943 (stellar, $q = 0$). Cluster galaxies: 17238, 17159, 17276
D	Holes	133	2AB-B	00 14 28.97	15 44 14.0	a	8000	QSO candidate: 14455 ($z = 0.545, q = 6$)
E	Holes	134	3AB-A	00 13 55.82	15 41 51.0	a	10000	Radio sources: 12887 (outside catalog, $q = 1$), 12701 (outside catalog, $z = 0.5124, q = 6$). QSO candidate: 12916 ($z = 0.418, q = 4$)
F	Holes	134	3AB-B	00 13 55.82	15 34 51.0	a	10000	QSO candidate: 8846 ($z = 0.242, q = 6$)
G	Holes	135	4AB-A	00 15 05.66	15 52 32.0	a	11000	QSO candidate: 17418 ($z = 0.553, q = 6$). Radio source: 54W052 (outside catalog, $q = 0$)
H	Holes	135	4AB-B	00 15 05.66	15 45 32.0	a	11000	QSO candidate: 14959 ($z = 1.067, q = 4$)
I	Holes	261	22AB-A	00 14 35.86	15 52 26.0	c	10500	Partially retarget C
J	Holes	261	22AB-B	00 14 47.08	15 42 32.0	c	10500	Radio source: (misidentified, no spectrum obtained). QSO candidate: 14524 ($q = 1$)
K	Holes	263	27A	00 14 47.92	15 29 48.0	c	16000	QSO candidate: 6403 ($z = 0.468, q = 4$)
L	Slits	...	4B	00 15 08.40	15 46 10.1	c	8000	Partially retarget H
M	Slits	...	5A	00 15 50.81	15 42 43.3	c	18000	Radio source: 12487 (outside catalog, $z = 0.544, q = 4$)
N	Slits	...	21A	00 14 25.87	15 31 50.3	c	20000	Retarget A
O	Slits	...	22B1	00 14 47.08	15 42 35.1	c	37000	Retarget J
P	Slits	7	322A	00 14 35.86	15 54 00.0	e	3000	Partially retarget I
Q	Slits	112	422A	00 14 35.86	15 53 30.0	g	6000	Partially retarget I
R	Slits	118	43A	00 13 52.97	15 42 10.0	(g), j	6000	Retarget E
S	Slits	119	43B	00 13 56.30	15 34 47.5	(g), j	6000	Retarget F
T	Slits	123	45A	00 15 53.84	15 41 37.2	g	6000	Partially retarget M. Bright galaxy: 11746. QSO candidate: 11973 ($q = 1$)
U	Slits	218	522A	00 14 35.86	15 52 30.0	j	6864	Retarget I
V	Slits	221	B68B	00 15 45.13	15 29 13.0	j	3000	Bright galaxies: 5799, 3873
W	Slits	222	B68C	00 15 23.10	15 31 26.0	j	4000	Bright galaxies: 6517, 6024
X	Slits	223	B68D	00 14 46.55	15 31 27.9	j	2000	Retarget K
Y	Slits	225	B68F	00 14 17.73	15 38 55.0	j	2000	Bright galaxies: 10081, 11790
Z	Slits	226	B68G	00 14 38.50	15 38 08.5	j	2000	Bright galaxies: 11651, 9290, 11277
AA	Slits	227	B68H	00 15 18.00	15 38 00.0	j	3000	Bright galaxy: 11514. QSO candidate: 9640 ($z = 0.729, q = 3$)
BB	Slits	228	B68I	00 15 39.00	15 42 00.0	j	4000	Bright galaxies: 13576, 14054, 12006
CC	Slits	229	B68J	00 14 14.00	15 44 20.0	j	2500	Bright galaxies: 13536, 14206
DD	Slits	230	B68K	00 14 26.40	15 48 55.0	j	2000	Bright galaxies: 16664, 16360. Partially retarget C
EE	Slits	231	B68L	00 14 47.00	15 50 30.0	j	1000	Bright galaxy: 17710. Partially retarget C and Q
FF	Slits	429	C68A	00 15 30.00	15 33 43.9	n	3858	Partially retarget W. Bright galaxies: 9171, 8564, 6952, 6471. QSO candidates: 8794 (star, $q = 6$), 7225 ($q = 0$)
GG	Slits	434	C68F	00 15 37.00	15 44 30.0	n	2500	Bright galaxies: 15295, 13673. UV-excess galaxy: 15592. QSO candidates: 14860 ($z = 0.979, q = 4$), 13557 (star, $q = 2$), 13318 (star, $q = 6$), 12920 (star, $q = 5$)
C. Herc 1 Multiaperture Masks								
A	Holes	235	1AB-A	17 20 32.13	49 57 24.2	b	4000	Radio sources: 9236, 10292, 9773 (stellar, $z = 0.924, q = 3$)
B	Holes	235	1AB-B	17 19 43.86	49 52 31.4	b	4000	Radio source: 6549. QSO candidate: 7345 ($z = 1.042, q = 3$)
C	Holes	236	2AB-A	17 17 25.20	50 01 06.2	b	4000	Radio source: 12010. QSO candidate: 11353 ($z = 1.293, q = 3$)
D	Holes	236	2AB-B	17 18 17.25	50 01 24.2	b	4000	Radio source: 12136
E	Holes	237	3AB-A	17 19 33.07	49 44 47.5	b	5000	Radio sources: 1742, 3886 (stellar, $z = 2.158, q = 5$)
F	Holes	237	3AB-B	17 18 54.88	49 45 04.2	b	4000	QSO candidate: 2441 ($z = 1.390, q = 4$)
G	Holes	238	4AB-A	17 18 54.31	50 19 31.2	b	6000	Radio source: 53W071 (outside catalog, $z = 0.287, q = 4$)
H	Holes	238	4AB-B	17 20 00.96	50 13 29.3	b	6000	Radio source: 17210
I	Holes	239	5AB-A	17 17 43.89	49 52 24.6	b	4000	QSO candidate: 6612 ($z = 1.381, q = 5$)
J	Holes	239	5AB-B	17 18 07.46	49 47 31.8	b	4000	Radio source: 3961 (stellar, $q = 0$)
K	Slits	194	H1A2	17 20 34.13	49 57 02.0	i	2300	Retarget A
L	Slits	195	H2A2	17 17 29.00	50 00 45.0	(i), l	3500	Retarget C
M	Slits	196	H3A2	17 19 32.00	49 45 00.0	(i), l	4000	Retarget E
N	Slits	197	H4B2	17 20 01.38	50 13 38.1	i, j	8931	Retarget H
O	Slits	198	H4B3	17 20 01.20	50 14 00.0	(i), j	3000	Retarget H
P	Slits	199	H5A2	17 17 43.01	49 52 24.0	(i), j	4000	Retarget I
Q	Slits	215	BHER1B	17 19 46.84	49 52 06.5	(j), l	4000	Retarget B
R	Slits	216	BHER4A	17 18 50.01	50 19 31.2	(j), l	4000	Retarget G
S	Slits	217	BHER5B	17 18 07.54	49 47 31.2	j	3000	Retarget J
T	Slits	269	HERC1A3	17 20 34.00	49 56 30.0	l	6000	Retarget A
U	Slits	270	HERC2B2	17 18 17.00	50 01 50.0	l	4700	Retarget D
V	Slits	360	HERC1QB	17 19 16.58	49 52 25.0	m	4000	QSO candidates: 7440 (star, $q = 3$), 7334 ($z = 0.739, q = 5$), 7087 ($q = 1$)
W	Slits	362	HERC1QD	17 17 22.81	49 49 25.3	m	2000	QSO candidates: 4305 ($z = 1.454, q = 2$), 6421 ($q = 0$)

TABLE 5—Continued

Sequence (1)	Type (2)	KPNO (3)	ID (4)	α_{1950} (5)	δ_{1950} (6)	Runs (7)	T (8)	Special Targets (9)
X	Slits	366	HERC1QH	17 18 17.71	50 13 13.0	m	3000	QSO candidates: 17039 ($q = 0$), 16924 ($q = 0$), 16113 ($q = 0$), 17789 ($q = 0$), 16378 ($q = 0$), 17409 ($z = 0.360$, $q = 6$)
Y	Slits	368	HERC1QJ	17 17 29.81	49 41 57.0	m	3097	QSO candidates: 2035 ($q = 0$), 735 (star, $q = 4$), 1032 ($z = 2.597$, $q = 6$), outside catalog ($q = 0$). UV-excess galaxies: 2287, 1917, 1438, 22
D. Lynx 2 Multiaperture Masks								
A	Slits	145	LYNX2A85	8 43 06.48	44 39 54.0	h, k	27000	Radio sources: 4453 (stellar, $z = 1.141$, $q = 5$), 4406, 4723
B	Slits	346	LYNX2QB	8 40 22.92	44 46 12.4	m	3000	QSO candidates: 6689 ($q = 1$), 6410 (star, $q = 6$), 6124 ($z = 3.187$, $q = 6$)
C	Slits	347	LYNX2QC	8 42 24.95	44 54 47.0	m	3000	QSO candidates: 8450 (star, $q = 5$), 8991 ($z = 2.321$, $q = 6$), 9971 ($z = 2.253$, $q = 6$). NELG candidate: 9398
D	Slits	349	LYNX2QE	8 40 42.00	44 51 35.0	m	1200	QSO candidate: 8363 ($z = 1.334$, $q = 5$). UV-excess galaxy: 8862. NELG candidate: 8946
E	Slits	351	LYNX2QG	8 40 30.62	44 58 51.7	m	2104	QSO candidates: 10671 ($z = 0.359$, $q = 6$), 11071 ($q = 0$). UV-excess galaxy: 11699. NELG candidates: 10197, 11447
F	Slits	355	LYNX2QL	8 43 16.54	44 51 17.0	m	4000	QSO candidates: 7120 ($z = 0.891$, $q = 3$), 7768 ($q = 0$), 8681 (star, $q = 4$)

Col. (1).—Sequence number, by which it is identified throughout the paper.

Col. (2).—Type of apertures.

Col. (3).—KPNO serial number.

Col. (4).—Authors' identifier.

Col. (5).—Right ascension in hours, minutes, and seconds of mask center (1950 equinox).

Col. (6).—Declination in degrees, arcminutes, and arcseconds of mask center (1950 equinox).

Col. (7).—Observing runs during which the mask was observed. The mask was originally created for the first run in the list. If the first run is parenthesized, then it was not observed during that run, although it was created for that run.

Col. (8).—Total exposure time in seconds.

Col. (9).—List of special targets.

observing time was devoted to the B_J -limited sample in SA 57 than to the R_F -limited sample. Of the 14 objects in the R_F -limited sample in SA 57 that lack acceptable redshifts, 12 were observed once in poor conditions, and two were never observed. All 14 are red ($B_J - R_F > 1$), which is expected because the bluer objects appear in the B_J -limited sample. Herc 1 is 90% complete for both $R_F \leq 18.5$ and $B_J \leq 19.5$, dropping to 74% and 86% complete for $R_F \leq 19$ and $B_J \leq 20$, respectively. Most of the spectra for the Lynx 2 bright samples were obtained during one Nessie run under good observing conditions, making it the most homogeneous sample in the entire survey. It is 89% and 94% complete for $R_F \leq 18$ and $B_J \leq 19$, respectively. Its completeness drops to 74% and 79% for $R_F \leq 18.5$ and $B_J \leq 19.75$, respectively.

A number of the brightest objects lacking acceptable redshifts have been observed spectroscopically only under poor conditions. These objects tend to have intermediate colors, while acceptable redshifts were obtained for objects of similar magnitude but more extreme colors observed at the same time. This pattern is also seen at the faint limit of the bright samples in both Herc 1 and Lynx 2. Figure 3 plots the distribution in $B_J - R_F$ of those objects in Herc 1 and Lynx 2 in the magnitude range $18 < R_F \leq 19$ that have been observed spectroscopically, split into those with and without acceptable redshifts. Those lacking acceptable redshifts are distributed in a narrower range of $B_J - R_F$ color. This is readily understood: at a given spectral signal-to-noise ratio, blue objects are more likely to have detectable emission lines and red objects are more likely to have strong absorption lines and continuum breaks, while those with intermediate colors have the weakest features. Hence attention must be paid to color biases when extending the Herc 1 and Lynx 2 bright samples to their faintest limits.

In summary, combined over all four fields, the bright

photometric R_F -limited sample contains 473 extended objects for $R_F \leq 19$, of which 335, or 71%, have reliable redshifts ($q > 2$). Seven of these were found spectroscopically to be misclassified stars. The distribution of the remaining 328 reliable galaxy redshifts has a median redshift of 0.142. The bright B_J -limited sample contains 336 extended objects for $B_J \leq 20$, of which 285, or 85%, have reliable redshifts. Five of these are misclassified stars. The distribution of the 280 reliable galaxy redshifts has a median redshift of 0.123. There are 321 objects in common between the bright R_F -limited and bright B_J -limited photometric samples, of which 276 have reliable redshifts.

4.4. Faint Statistical Sample

Each multihole and multislit aperture mask defines a separate sample of galaxies, which hereafter we will call the “statistical sample” for the mask, consisting of all galaxies targeted by that mask, excluding those galaxies that are special targets of the mask or that were targeted by a previously created mask. If all galaxies within the statistical sample and brighter in R_F than a special target yield a reliable redshift ($q > 2$), then the special target is regarded as part of the statistical sample. If a galaxy is targeted by more than one mask, it belongs to the statistical sample of the mask that first targeted it. The “survey statistical sample” consists of the union of the statistical samples for each multiaperture mask.

Different algorithms may be used to extract well-defined, statistically complete subsamples of the survey statistical sample. Columns (10)–(13) in Table 6 provide the necessary information to support a number of such algorithms. Column (10) lists the sources of the redshifts for each object. A capital letter indicates that the object was observed in a multiaperture mask, and may be cross-referenced with column (1) in Table 5 to determine which mask. A lowercase

TABLE 6—Continued

N_{ser} (1)	α_{1950} (2)	δ_{1950} (3)	R_F (4)	$U - B_J$ (5)	$B_J - R_F$ (6)	$R_F - I_N$ (7)	z (8)	q (9)	Source (10)	N_a (11)	N_b (12)	Notes (13)
117345.....	13 06 30.65	29 50 06.0	20.48	0.79	2.09	1.10	...	0	KK	
101834.....	13 05 27.98	29 25 41.1	20.49	-0.82	0.56	0.67	0.3079	6	DD	10	0	
104141.....	13 05 41.51	29 29 48.0	20.51	0.23	0.73	0.70	...	0	K, R	
118740.....	13 05 46.08	29 52 33.5	20.53	1.25	1.85	0.93	0.3975	6	Z, Z	0	0	
105434.....	13 05 46.69	29 31 52.2	20.57	0.28	0.89	1.63	...	0	K, I, R	
107214.....	13 06 36.62	29 34 38.3	20.57	-0.31	1.66	1.64	...	0	C, P, o	
115148.....	13 06 01.17	29 46 32.4	20.62	0.51	1.68	1.07	...	0	NN	X
104621.....	13 05 42.14	29 30 33.9	20.67	1.69	1.92	1.20	0.4041	1	I	
103864.....	13 05 31.90	29 29 20.1	20.71	-0.19	1.37	1.29	0.4669	6	I, S	2	2	
107491.....	13 06 39.41	29 35 03.1	20.73	0.35	1.55	1.04	0.3342	6	E, P	5	0	
109972.....	13 07 20.38	29 38 39.5	20.73	-0.16	1.06	0.74	...	0	AA	
105459.....	13 05 42.70	29 31 54.6	20.77	0.24	1.54	0.85	...	0	S	
104776.....	13 05 41.80	29 30 47.9	20.78	1.75	1.83	1.16	0.4033	6	S	4	1	
106018.....	13 05 26.84	29 32 47.4	20.79	-0.02	0.72	0.94	...	0	S	
110894.....	13 07 22.99	29 40 04.2	20.80	0.42	1.56	0.82	...	0	A, AA, o	
101796.....	13 05 41.42	29 25 35.2	20.82	-0.51	0.61	0.63	...	0	DD	
105558.....	13 05 30.46	29 32 04.1	20.86	-0.40	0.90	0.75	0.3859	6	I, K, R	4	2	
118532.....	13 05 30.90	29 52 08.5	20.88	-0.30	0.85	0.03	0.2261	6	M	C
111379.....	13 07 27.00	29 40 50.7	20.89	1.73	1.64	1.01	...	0	A, AA	
104045.....	13 05 23.87	29 29 41.3	20.93	1.12	2.28	1.62	...	0	S	
104064.....	13 05 32.65	29 29 41.7	20.94	-0.27	0.89	1.00	...	0	K	
119199.....	13 05 36.80	29 53 29.3	20.94	-0.34	1.08	0.51	...	0	N, Z, Z	
110420.....	13 05 18.51	29 39 23.0	20.94	-0.35	1.38	0.80	...	0	G	
118710.....	13 05 28.30	29 52 28.0	20.96	-0.25	1.00	0.65	0.3158	5	N	1	1	
103253.....	13 05 31.55	29 28 19.8	20.99	-0.31	0.92	1.13	...	0	I	
105067.....	13 06 44.59	29 31 16.4	21.04	0.00	1.11	0.85	...	0	E, P	
106445.....	13 06 45.81	29 33 27.5	21.05	0.81	1.54	1.13	...	0	P	
110249.....	13 07 19.05	29 39 05.1	21.18	-0.25	0.87	0.70	0.2901	6	A	7	3	
111349.....	13 07 18.43	29 40 48.4	21.19	-0.37	1.08	0.90	...	0	AA	
117370.....	13 05 38.71	29 50 07.4	21.19	-0.23	1.12	-0.12	...	0	N, Z, Z	
110818.....	13 07 09.44	29 39 57.7	21.20	0.42	1.35	1.03	...	0	AA	
105448.....	13 05 40.90	29 31 54.0	21.20	0.46	1.45	0.77	...	0	X	J
106644.....	13 06 40.75	29 33 49.3	21.22	0.24	1.80	1.39	...	0	P	
104700.....	13 05 36.80	29 30 41.6	21.33	0.06	1.13	1.15	0.4004	4	K, R	11	3	
105946.....	13 05 37.07	29 32 40.7	21.33	1.17	1.62	1.23	...	0	I, X	J
104437.....	13 05 25.89	29 30 16.7	21.35	-0.35	0.78	1.35	...	0	K, R	
110637.....	13 05 33.77	29 39 42.8	21.35	-0.23	1.14	0.43	...	0	G	
118732.....	13 05 42.32	29 52 31.6	21.36	-0.55	0.96	0.59	0.8576	3	M, T	8	1	
118531.....	13 05 43.61	29 52 10.0	21.36	1.77	1.38	0.66	0.2245	3	N, Z, Z	6	2	
104259.....	13 05 40.52	29 30 00.2	21.37	-0.41	0.72	1.27	0.6014	4	S	11	3	
105050.....	13 05 37.94	29 31 16.2	21.38	0.38	0.55	0.63	...	0	I, R	
106273.....	13 06 46.06	29 33 10.2	21.39	-0.01	2.13	1.57	...	0	C	
100172.....	13 06 20.69	29 21 10.2	21.40	-0.71	0.91	1.42	...	0	v	
105769.....	13 05 48.66	29 32 23.5	21.44	-0.24	0.60	0.62	0.1217	6	X	10	0	J
106160.....	13 06 36.36	29 33 01.2	21.44	-0.03	0.78	1.15	0.6739	4	C	13	3	
118620.....	13 05 30.82	29 52 19.3	21.49	1.05	1.99	1.35	0.5150	2	N, Z, Z	
105585.....	13 05 35.22	29 32 06.1	21.53	-0.56	1.05	0.83	0.3315	6	I, S	16	5	
103605.....	13 05 30.01	29 28 53.2	21.54	-0.63	0.92	0.67	0.3924	6	K, S	16	4	
104745.....	13 05 45.07	29 30 44.8	21.69	0.58	1.14	1.56	...	0	K, R	
104389.....	13 05 34.71	29 30 12.3	21.75	-0.45	1.83	0.95	...	0	R	
118978.....	13 05 34.98	29 52 57.9	21.78	-3.90	1.14	0.46	0.7990	3	N	20	3	
105703.....	13 06 34.56	29 32 16.1	21.83	0.46	1.25	1.65	0.6733	3	C, P	18	3	
104460.....	13 05 42.43	29 30 17.3	21.83	-0.33	1.27	1.08	...	0	I	
104212.....	13 05 43.05	29 29 54.5	21.83	-0.31	0.70	0.72	...	0	K, R	
117895.....	13 05 41.79	29 51 03.2	21.86	-0.51	1.36	0.66	0.5197	6	N	24	3	
105321.....	13 06 47.04	29 31 41.9	21.86	0.57	1.15	0.80	0.4531	3	E, P	19	1	
110772.....	13 07 26.98	29 39 53.3	21.87	-0.30	1.15	0.53	...	0	A	
118593.....	13 05 34.56	29 52 16.2	21.89	-0.37	0.56	0.84	...	0	M, T, Z, Z	C
106028.....	13 05 29.32	29 32 48.4	21.89	-0.38	1.01	50.93	0.3860	4	I, R	25	6	
105169.....	13 05 37.12	29 31 27.6	21.91	-0.59	0.83	0.60	0.5976	4	S	24	3	
118054.....	13 05 46.78	29 51 18.2	21.92	1.92	0.81	0.22	...	0	N	
118671.....	13 05 44.07	29 52 26.4	21.93	-0.66	1.22	1.31	...	0	T	
118629.....	13 05 32.54	29 52 21.0	21.93	-0.90	1.84	1.36	0.5201	1	N	
105826.....	13 05 46.69	29 32 29.2	21.98	-0.47	0.67	0.43	...	0	X	J
110864.....	13 07 06.13	29 40 03.0	22.06	-0.68	0.77	0.26	0.3939	3	AA	X
105473.....	13 05 33.48	29 31 56.6	22.27	0.34	0.23	0.87	...	0	X	J
105636.....	13 05 31.08	29 32 11.5	22.31	0.12	0.55	1.07	...	0	X	
105921.....	13 05 42.41	29 32 38.2	22.32	-0.25	0.70	-0.36	...	0	X	J
104972.....	13 05 34.91	29 31 07.1	22.33	3.12	1.10	1.16	...	0	X	J
104998.....	13 05 50.52	29 31 09.6	22.35	-0.15	0.84	50.74	...	0	X	J
105590.....	13 05 44.28	29 32 06.0	23.87	0.28	-0.40	2.89	...	0	X	J

TABLE 6—Continued

N_{ser} (1)	α_{1950} (2)	δ_{1950} (3)	R_F (4)	$U - B_J$ (5)	$B_J - R_F$ (6)	$R_F - I_N$ (7)	z (8)	q (9)	Source (10)	N_a (11)	N_b (12)	Notes (13)
208230.....	0 13 54.01	15 34 41.2	20.42	0.03	0.88	0.85	0.2105	4	z	
211372.....	0 14 33.96	15 39 29.4	20.42	-0.28	1.03	0.39	0.3017	6	y	
205882.....	0 14 25.87	15 30 53.3	20.43	-0.11	1.55	1.34	...	0	A	
203841.....	0 14 36.43	15 27 24.5	20.43	0.36	2.37	1.26	0.5400	5	1	
212817.....	0 14 44.21	15 41 55.3	20.44	-0.23	1.28	0.61	0.3869	3	z	
214020.....	0 14 41.53	15 44 01.3	20.44	0.75	2.22	0.91	0.3947	5	O	2	-1	
201017.....	0 14 34.69	15 21 39.0	20.45	-0.14	0.83	0.47	0.2041	5	y	
205533.....	0 14 19.07	15 30 22.9	20.45	1.37	1.78	1.08	0.3082	2	N	
212019.....	0 13 58.42	15 40 38.0	20.46	-0.25	1.31	0.51	0.3570	6	E, R	3	0	
206261.....	0 15 47.63	15 31 25.4	20.46	0.32	1.29	0.84	...	0	z	
212831.....	0 14 44.21	15 41 56.8	20.46	-0.24	1.29	0.61	...	0	z	
207620.....	0 15 07.16	15 33 37.6	20.46	-0.10	1.13	0.66	0.5360	4	y	
207308.....	0 15 50.77	15 33 06.1	20.47	0.48	0.66	0.07	...	0	z	
212737.....	0 15 09.81	15 41 46.4	20.47	-0.35	1.48	0.88	...	0	z	
201853.....	0 14 18.72	15 23 33.8	20.47	-0.44	1.38	0.33	...	0	B	
210790.....	0 14 16.88	15 38 36.1	20.47	0.06	0.96	0.65	0.0927	3	y	
210947.....	0 15 39.36	15 38 45.6	20.47	0.08	1.00	0.70	0.3021	6	y	
201670.....	0 14 54.27	15 23 05.8	20.48	-0.23	1.52	0.67	0.2978	4	z	
201585.....	0 15 04.87	15 22 54.2	20.48	0.14	0.97	0.57	0.1719	4	y, z	
208538.....	0 13 58.78	15 35 10.0	20.48	-0.05	1.02	0.53	0.1594	1	y, z	
210700.....	0 15 31.06	15 38 24.0	20.48	0.03	0.89	0.56	0.2542	4	y, z	
208178.....	0 15 17.71	15 34 31.0	20.48	0.08	1.06	0.35	0.0801	6	y	
203622.....	0 14 12.08	15 27 04.7	20.49	0.00	0.75	0.51	0.0282	6	y, z	
209309.....	0 15 46.23	15 36 16.3	20.49	-0.02	1.09	0.43	0.2065	6	y	
212212.....	0 13 49.83	15 40 56.5	20.49	0.73	1.86	1.39	0.5123	4	E, R	3	0	
215671.....	0 15 29.37	15 47 07.1	20.50	0.00	1.01	0.88	...	0	y	
213851.....	0 15 48.28	15 43 36.5	20.50	0.28	1.03	0.71	...	0	y	
212002.....	0 15 54.71	15 40 29.1	20.51	0.09	0.96	0.46	0.1405	6	T	1	0	
214352.....	0 15 39.45	15 44 29.5	20.51	0.29	0.95	0.63	0.1488	5	y, z	
213957.....	0 14 54.66	15 43 54.8	20.51	1.17	1.80	0.81	...	0	J	
201320.....	0 14 50.81	15 22 22.1	20.51	-0.20	1.01	0.46	0.3513	4	y	
208625.....	0 15 59.14	15 35 11.1	20.52	-0.01	0.55	0.36	0.0257	6	y	
213100.....	0 15 28.00	15 42 23.9	20.52	-0.03	0.92	0.34	0.2603	5	y	
207703.....	0 14 30.77	15 33 47.8	20.52	0.62	2.05	0.85	...	0	A, N	
207404.....	0 15 37.30	15 33 14.3	20.53	-0.00	1.18	0.81	...	0	z	
201618.....	0 15 21.09	15 22 58.2	20.54	0.15	0.96	0.88	0.2098	4	y, z	
202606.....	0 14 36.95	15 25 01.7	20.54	-0.32	0.86	0.40	0.2976	6	B	1	1	
205935.....	0 15 06.14	15 30 55.5	20.56	-0.44	0.83	0.37	0.3038	6	u	
202759.....	0 15 14.33	15 25 16.8	20.56	1.62	0.74	0.94	...	0	j	
206070.....	0 14 57.54	15 31 07.7	20.57	-0.16	1.10	0.70	0.4101	3	z	
209122.....	0 14 05.44	15 36 05.4	20.57	0.50	1.49	0.90	0.0000	3	F, u	2	0	
214432.....	0 15 15.78	15 44 43.7	20.57	-0.43	1.08	0.94	0.6199	4	H, L	2	-1	
216715.....	0 14 23.15	15 49 25.3	20.57	-0.13	0.52	-2.08	...	0	y, z	
213323.....	0 14 40.55	15 42 48.8	20.58	-0.32	1.50	0.89	0.3950	6	O	2	0	
213603.....	0 15 34.49	15 43 14.0	20.58	-0.08	1.09	0.88	...	0	z	
206622.....	0 14 47.37	15 32 00.9	20.58	0.60	1.57	0.85	...	0	K	
206451.....	0 15 08.52	15 31 42.5	20.58	0.12	1.00	0.47	...	0	y, z	
208222.....	0 13 59.76	15 34 39.3	20.59	-0.25	0.30	0.37	0.0141	6	S, u	2	0	
217281.....	0 15 11.76	15 50 47.4	20.59	0.08	1.67	0.99	0.5273	3	G, u	0	-1	
215582.....	0 15 13.49	15 46 57.6	20.60	0.60	1.97	1.26	0.4340	3	H	2	-1	
202489.....	0 15 03.27	15 24 46.2	20.60	0.18	1.02	0.98	0.2500	2	y	
208292.....	0 14 07.05	15 34 45.4	20.61	0.35	0.82	0.57	0.0982	3	y, z	
203518.....	0 14 48.64	15 26 47.1	20.61	-0.21	1.10	0.52	...	0	z	
206074.....	0 14 45.01	15 31 08.8	20.61	0.06	0.57	0.51	...	0	z	
213145.....	0 14 38.62	15 42 31.8	20.62	0.28	2.21	1.09	...	0	O	
210276.....	0 15 26.48	15 37 45.0	20.62	-0.03	1.37	0.72	...	0	z	
213098.....	0 15 41.02	15 42 22.2	20.63	-0.34	1.30	0.86	...	0	M	
200648.....	0 14 57.96	15 20 37.5	20.64	0.06	0.80	0.12	0.3925	1	y, z	
217573.....	0 14 42.15	15 51 32.2	20.64	-0.28	0.90	0.71	0.2599	6	U	0	-1	
204211.....	0 15 15.97	15 28 04.3	20.65	-0.12	0.88	0.23	0.1721	3	y	
215791.....	0 15 09.11	15 47 24.1	20.65	0.55	1.88	1.18	0.3777	4	L	2	0	
205044.....	0 14 41.91	15 29 33.5	20.65	-0.11	1.25	0.95	...	0	z	
205108.....	0 14 42.66	15 29 39.8	20.66	-0.20	0.92	0.27	0.0240	2	y	
207171.....	0 15 16.59	15 32 51.9	20.66	-0.39	1.10	0.73	...	0	z	
209360.....	0 15 56.14	15 36 20.2	20.67	-0.36	1.18	0.65	0.3900	2	z	
209105.....	0 14 45.71	15 36 01.8	20.67	-0.29	0.66	0.49	0.8033	3	y	
212261.....	0 15 47.69	15 40 56.2	20.68	0.62	1.05	0.67	...	0	M	
212438.....	0 13 52.25	15 41 17.9	20.69	0.24	0.89	0.34	...	0	E, u, y, z	
206548.....	0 15 41.33	15 31 51.2	20.69	-0.59	1.17	0.89	...	0	z	
208107.....	0 14 02.23	15 34 26.9	20.69	0.16	1.83	1.03	...	0	F, S	
210011.....	0 13 58.93	15 37 30.0	20.69	-0.31	0.80	0.62	0.3456	5	y	
209728.....	0 15 34.63	15 36 59.3	20.70	-0.19	1.18	0.35	0.3874	6	z	

TABLE 6—Continued

N_{ser} (1)	α_{1950} (2)	δ_{1950} (3)	R_F (4)	$U - B_J$ (5)	$B_J - R_F$ (6)	$R_F - I_N$ (7)	z (8)	q (9)	Source (10)	N_s (11)	N_b (12)	Notes (13)
205637.....	0 15 13.65	15 30 29.4	20.71	-0.22	1.01	1.09	0.3043	2	z	
204944.....	0 13 54.28	15 29 28.8	20.72	-0.01	0.60	-0.27	0.1155	5	y, z	
203621.....	0 14 17.41	15 27 03.9	20.72	-0.53	0.76	0.64	0.4566	5	y	
206661.....	0 15 17.33	15 32 02.6	20.73	0.07	0.99	0.21	0.1908	3	z	
211699.....	0 15 37.21	15 40 01.6	20.73	0.20	1.12	0.88	0.2618	3	z	
208214.....	0 13 59.58	15 34 38.6	20.74	-0.32	0.22	0.62	0.0146	6	S	2	0	
211684.....	0 14 27.66	15 40 04.1	20.74	-0.14	0.89	0.41	0.1750	6	y, z	
209956.....	0 14 25.97	15 37 24.6	20.75	0.05	0.69	0.35	0.0929	6	y	
203018.....	0 14 12.40	15 25 52.6	20.75	-0.10	1.00	0.61	0.4671	2	z	
200766.....	0 14 52.95	15 20 57.6	20.76	0.01	0.80	0.51	0.3505	5	y	
203062.....	0 14 36.54	15 25 54.1	20.77	0.70	1.72	0.63	...	0	B	
205933.....	0 15 28.29	15 30 55.1	20.78	-0.05	1.14	0.27	0.2822	3	z	
214245.....	0 14 57.50	15 44 23.1	20.78	-0.36	1.36	0.16	0.2339	4	H, u	3	-1	
201941.....	0 14 59.40	15 23 42.4	20.78	-0.08	0.96	0.60	0.2485	5	z	
215363.....	0 15 26.24	15 46 27.3	20.79	-0.02	0.97	0.77	0.3600	3	z	
205410.....	0 14 39.09	15 30 09.2	20.79	-0.10	1.19	0.42	0.2506	5	z	
206989.....	0 14 14.16	15 32 37.2	20.79	0.02	1.20	0.74	...	0	z	
202590.....	0 14 40.30	15 24 59.6	20.80	-0.21	1.00	0.60	0.4584	4	z	
211919.....	0 14 33.67	15 40 27.0	20.80	-0.40	1.19	0.58	...	0	z	
210454.....	0 15 13.36	15 38 01.9	20.81	-0.40	1.06	0.43	0.3925	2	z	
202789.....	0 15 33.35	15 25 20.9	20.81	0.42	0.62	0.35	0.0000	2	y, z	
211412.....	0 13 56.22	15 39 33.0	20.82	0.01	0.66	0.38	0.0693	5	E, y	5	1	
208767.....	0 14 03.41	15 35 31.5	20.83	-0.31	1.57	0.93	...	0	F	
205023.....	0 14 20.25	15 29 32.6	20.83	0.18	1.16	0.22	0.2109	3	z	
213200.....	0 14 20.37	15 42 37.5	20.84	1.58	1.72	1.04	...	0	D	
215344.....	0 15 17.44	15 46 25.9	20.84	-0.30	1.45	1.21	...	0	L	
206639.....	0 15 22.12	15 32 00.6	20.84	-0.05	1.02	0.65	...	0	z	
207927.....	0 14 28.87	15 34 08.0	20.84	1.45	1.76	0.92	...	0	A	
207475.....	0 14 53.36	15 33 22.7	20.88	-0.48	0.09	0.89	...	0	y, z	
216094.....	0 15 26.68	15 47 56.2	20.88	0.10	0.85	0.65	0.1586	4	z	
213682.....	0 15 29.63	15 43 23.5	20.89	0.14	1.03	0.06	0.2901	3	z	
206987.....	0 15 29.24	15 32 33.1	20.89	-0.14	0.93	-0.27	0.1706	6	z	
206438.....	0 14 34.46	15 31 43.3	20.90	0.80	1.82	1.18	...	0	N	
207970.....	0 15 19.36	15 34 09.8	20.91	0.12	0.74	0.36	...	0	z	
215070.....	0 15 18.69	15 45 54.5	20.91	0.27	0.84	0.59	0.0835	2	z	
209708.....	0 14 47.66	15 36 59.8	20.91	-0.03	0.88	0.36	...	0	z	
210442.....	0 15 51.48	15 37 58.3	20.91	-0.44	0.77	0.26	0.3140	6	z	
209576.....	0 14 52.54	15 36 45.0	20.91	-0.08	0.82	-0.07	0.0473	1	z	
202869.....	0 14 27.76	15 25 32.4	20.93	0.37	1.61	1.40	0.5440	4	B, u	3	2	
210502.....	0 14 15.42	15 38 09.1	20.93	-0.09	1.01	0.83	0.5189	2	z	
212906.....	0 14 28.93	15 42 05.3	20.94	0.31	1.53	0.54	...	0	D	
206570.....	0 15 38.55	15 31 54.1	20.94	0.10	1.07	0.73	...	0	v	
207650.....	0 14 10.63	15 33 44.1	20.95	0.04	0.58	0.89	...	0	z	
203243.....	0 15 12.58	15 26 15.1	20.95	-0.03	0.69	0.71	0.2045	5	y	
207915.....	0 14 52.96	15 34 05.4	20.95	-0.20	0.78	0.43	0.4101	1	z	
214803.....	0 14 47.28	15 45 27.5	20.97	0.00	0.61	0.43	...	0	y	
212319.....	0 14 47.03	15 41 06.6	21.00	0.65	2.02	1.31	...	0	J	
205047.....	0 15 30.50	15 29 32.4	21.00	-0.20	0.99	0.18	0.2092	2	z	
212965.....	0 15 40.26	15 42 06.8	21.00	0.08	0.82	0.77	...	0	z	
216261.....	0 14 40.87	15 48 20.3	21.00	-0.07	0.75	0.53	0.1610	4	z	
211925.....	0 14 43.80	15 40 27.4	21.01	-0.27	1.09	0.59	0.5172	3	J, O	4	2	
215592.....	0 15 35.64	15 46 56.1	21.03	-0.48	1.23	0.86	0.3936	6	GG	8	0	U
210820.....	0 15 58.25	15 38 31.6	21.04	0.19	0.83	0.35	...	0	z	
207127.....	0 14 31.73	15 32 49.5	21.05	0.15	1.10	1.10	...	0	N	
201728.....	0 14 29.57	15 23 15.8	21.06	-0.23	1.12	0.24	0.6255	3	B	4	2	
201557.....	0 14 26.09	15 22 53.7	21.06	-0.39	1.11	1.15	...	0	B	R
202853.....	0 15 27.20	15 25 27.8	21.06	-0.27	0.82	0.13	0.3650	4	z	
207014.....	0 14 21.79	15 32 38.7	21.07	0.36	1.93	1.49	0.5553	6	N	11	4	
213515.....	0 14 56.25	15 43 08.5	21.10	0.15	0.76	0.33	0.0849	1	z	
214460.....	0 14 45.39	15 44 48.8	21.12	-0.02	1.59	1.09	...	0	J	
205523.....	0 14 25.10	15 30 21.9	21.12	-0.04	1.42	0.80	...	0	u	
206854.....	0 14 20.51	15 32 24.0	21.13	1.62	1.25	1.11	...	0	N	
217631.....	0 14 34.42	15 51 41.6	21.14	0.36	1.64	1.34	...	0	U	
208624.....	0 14 02.97	15 35 17.1	21.15	-0.69	1.26	1.04	0.6258	3	F	4	2	
201959.....	0 14 41.77	15 23 45.3	21.16	-0.33	0.66	0.66	0.2979	5	z	
204848.....	0 15 08.66	15 29 12.6	21.16	0.09	0.78	0.56	0.0683	6	z	
210201.....	0 15 28.93	15 37 39.3	21.16	0.79	0.44	0.75	...	0	y	
204911.....	0 14 25.99	15 29 22.0	21.18	0.07	1.29	0.92	...	0	A	
211758.....	0 13 48.59	15 40 10.9	21.19	0.24	0.44	0.94	...	0	y, z	
217651.....	0 15 03.25	15 51 43.5	21.21	1.67	1.55	1.03	...	0	G	
206715.....	0 14 20.51	15 32 10.7	21.22	0.01	1.07	1.10	0.5524	3	A	16	5	
205045.....	0 13 59.45	15 29 38.2	21.22	-0.07	0.75	0.25	...	0	z	

TABLE 6—Continued

N_{ser} (1)	α_{1950} (2)	δ_{1950} (3)	R_F (4)	$U - B_J$ (5)	$B_J - R_F$ (6)	$R_F - I_N$ (7)	z (8)	q (9)	Source (10)	N_s (11)	N_b (12)	Notes (13)
202484.....	0 15 31.98	15 24 46.1	21.23	-0.25	0.68	1.02	0.7185	4	z	
211386.....	0 15 42.40	15 39 25.9	21.24	-0.05	0.74	0.38	0.0933	6	z	
208607.....	0 14 14.87	15 35 15.3	21.26	-0.21	0.71	0.05	...	0	z	
213720.....	0 14 38.46	15 43 30.7	21.28	0.07	-0.06	0.98	...	0	y, z	
217679.....	0 14 44.66	15 51 50.0	21.29	-0.78	1.44	1.17	...	0	I	
207364.....	0 14 25.63	15 33 14.0	21.30	-0.65	0.51	0.84	...	0	z	
204867.....	0 15 08.66	15 29 14.8	21.30	0.24	0.50	0.84	...	0	z	
202162.....	0 14 37.43	15 24 10.2	21.33	1.84	1.62	1.20	...	0	B	
213278.....	0 14 46.93	15 42 44.8	21.35	-0.28	1.03	0.93	0.5471	3	J	16	3	
211623.....	0 13 57.37	15 39 55.9	21.38	-0.30	1.17	1.25	...	0	E	
217238.....	0 14 25.67	15 50 42.1	21.38	-0.23	0.93	-0.28	...	0	C, q, s, t	C
217500.....	0 14 34.51	15 51 21.3	21.42	0.21	0.97	0.96	...	0	C	
211929.....	0 14 00.03	15 40 28.4	21.43	-0.31	1.11	0.82	...	0	R	
207808.....	0 14 06.13	15 33 58.5	21.44	0.29	1.23	1.10	...	0	F	
217671.....	0 15 01.03	15 51 47.3	21.52	-0.03	1.61	1.00	...	0	G	
217159.....	0 14 24.27	15 50 29.7	21.53	-0.55	1.51	0.53	...	0	C	C
206655.....	0 13 58.02	15 32 07.8	21.54	0.25	0.33	49.97	...	0	z	
208293.....	0 14 05.38	15 34 45.5	21.58	-0.23	0.53	0.90	0.2307	5	S	10	0	
214037.....	0 14 30.64	15 44 03.7	21.59	0.33	2.10	1.04	0.5400	1	D, u	
212403.....	0 15 52.00	15 41 08.1	21.59	0.05	1.22	0.29	...	0	M	
215171.....	0 15 06.55	15 46 06.4	21.60	-0.60	1.12	0.97	...	0	L	
212235.....	0 15 55.23	15 40 52.9	21.64	0.24	0.81	1.24	...	0	M	
212202.....	0 15 49.83	15 40 48.9	21.67	1.95	1.42	1.22	...	0	M	
217739.....	0 15 00.85	15 51 58.6	21.71	-51.8	1.51	1.47	...	0	G	
208288.....	0 14 01.20	15 34 45.8	21.71	-0.32	0.51	0.72	0.7269	3	F, S	14	3	
214967.....	0 15 02.77	15 45 45.0	21.71	-0.42	1.02	1.00	...	0	L	
202922.....	0 14 22.64	15 25 38.9	21.75	-0.77	1.27	0.78	...	0	B	
217210.....	0 15 01.46	15 50 36.9	21.77	-0.33	1.62	0.91	...	0	G	
217276.....	0 14 26.24	15 50 48.3	21.78	-0.30	0.81	1.26	...	0	C	C
213980.....	0 15 10.29	15 43 55.9	21.79	-0.71	1.00	0.59	...	0	H	
214198.....	0 15 01.74	15 44 18.4	21.80	1.13	1.46	0.65	...	0	L	
214296.....	0 15 13.62	15 44 27.0	21.83	0.26	1.33	1.68	...	0	L	
207318.....	0 15 50.32	15 33 06.4	21.83	0.97	-0.02	0.86	...	0	z	
215115.....	0 15 05.47	15 46 01.7	21.83	-0.58	1.03	1.56	...	0	L	
203002.....	0 14 32.73	15 25 47.9	21.84	-0.70	1.54	0.35	...	0	B	
208652.....	0 13 57.11	15 35 20.1	21.85	-0.74	1.37	-2.13	0.7691	3	F	17	3	
206158.....	0 14 31.33	15 31 18.7	21.85	0.64	2.19	0.94	...	0	A	
211289.....	0 14 05.29	15 39 21.9	21.89	-0.45	1.05	0.23	0.0000	4	s	
200862.....	0 15 06.79	15 21 12.8	21.95	-0.13	0.99	0.50	0.0255	4	c	
211228.....	0 14 03.14	15 39 15.6	22.01	0.14	-0.05	1.24	...	0	z	
214673.....	0 14 23.84	15 45 13.3	22.04	-0.41	1.11	-0.17	...	0	D	
203414.....	0 14 29.21	15 26 35.6	22.06	0.75	1.66	1.97	...	0	B	R
215190.....	0 14 59.36	15 46 09.2	22.10	-0.21	1.45	0.73	...	0	L	
206928.....	0 15 28.65	15 32 26.1	22.24	-0.23	1.14	0.79	...	0	W	
215064.....	0 15 11.34	15 45 54.9	22.26	-0.68	0.76	-0.31	...	0	L	
207906.....	0 13 52.10	15 34 08.9	22.28	0.04	1.03	0.89	...	0	S	
215630.....	0 15 04.14	15 47 03.6	22.28	-0.54	2.28	50.37	...	0	L	
212123.....	0 15 52.02	15 40 41.2	22.32	1.31	-0.61	1.90	...	0	z	

C. Herc 1 Catalog

308890.....	17 17 40.35	49 56 02.0	12.58	0.29	1.48	0.19	0.0030	6	b	
311857.....	17 17 58.19	50 01 36.1	13.95	0.50	1.72	0.38	0.0332	6	x	
311360.....	17 18 03.29	50 00 41.7	14.39	0.84	1.66	0.82	0.0333	6	x	
312479.....	17 19 20.01	50 02 41.5	15.11	0.39	1.25	0.78	0.0549	6	x	
301703.....	17 17 20.43	49 43 05.6	15.50	0.62	1.02	0.40	0.0242	6	y, 3	
316721.....	17 18 43.89	50 12 20.6	16.10	0.85	1.58	0.69	0.0850	6	x	
306689.....	17 18 57.64	49 51 47.6	16.20	0.56	1.17	0.82	0.0520	6	x	
309625.....	17 17 17.28	49 57 29.0	16.27	0.25	1.05	0.16	0.0240	3	x	
303414.....	17 20 12.54	49 45 44.8	16.61	0.48	1.28	0.91	0.1171	6	o	
315439.....	17 18 20.67	50 09 18.5	16.76	0.85	1.48	0.78	0.0843	6	o	
310463.....	17 17 18.24	49 59 06.2	16.83	0.39	1.36	0.68	0.1561	6	C	0	-1	
305009.....	17 20 31.58	49 48 28.1	16.83	0.43	1.01	0.83	0.0605	6	o, r	
307977.....	17 17 51.93	49 54 22.4	16.88	-0.12	0.62	-0.10	0.0034	6	I, P	0	-1	
312423.....	17 20 27.64	50 02 25.2	16.92	0.32	1.07	0.83	0.0849	6	o	
316215.....	17 19 05.47	50 11 05.5	17.04	1.04	1.58	0.86	0.1214	6	o	
317964.....	17 18 11.20	50 15 25.1	17.04	0.57	1.30	0.65	0.0753	3	X, o	0	-1	
317050.....	17 18 58.66	50 13 09.7	17.08	0.61	1.28	0.79	0.0840	6	o	
306357.....	17 20 00.66	49 51 01.4	17.10	0.84	1.45	0.85	0.1214	6	o	
315086.....	17 19 56.23	50 08 12.9	17.14	0.79	1.47	0.84	0.1095	6	x	
313616.....	17 19 47.78	50 05 02.2	17.15	0.91	1.42	0.91	0.0852	6	o	
310554.....	17 18 41.36	49 59 09.6	17.15	0.23	1.25	0.77	0.2265	6	o	

TABLE 6—Continued

N_{ser} (1)	α_{1950} (2)	δ_{1950} (3)	R_F (4)	$U - B_J$ (5)	$B_J - R_F$ (6)	$R_F - I_N$ (7)	z (8)	q (9)	Source (10)	N_g (11)	N_b (12)	Notes (13)
407963.....	8 42 48.00	44 51 14.0	20.21	0.04	1.11	0.43	...	0	z	
407528.....	8 41 41.98	44 49 47.1	20.22	0.67	0.58	0.30	0.7896	4	z	
411415.....	8 41 47.90	45 00 35.4	20.22	-0.27	1.08	0.39	0.2370	1	v	
401888.....	8 41 05.88	44 33 24.2	20.23	0.01	1.16	0.45	...	0	z	
403652.....	8 43 18.12	44 38 48.2	20.24	-0.05	0.94	-0.02	0.1279	4	z	
405084.....	8 41 09.97	44 42 32.6	20.26	-0.04	1.21	0.43	...	0	z	
402232.....	8 43 23.80	44 34 45.4	20.26	-0.23	1.00	-0.16	...	0	z	
405580.....	8 41 35.73	44 44 06.6	20.26	0.11	1.07	0.26	...	0	z	
407792.....	8 41 21.07	44 50 25.0	20.28	0.02	0.98	0.55	...	0	t	
408861.....	8 42 00.67	44 53 33.6	20.29	-0.55	1.30	0.41	...	0	z	
404501.....	8 40 03.39	44 40 31.6	20.30	-0.16	0.89	-0.10	0.1494	3	z	
406078.....	8 40 59.32	44 45 08.8	20.31	-0.30	1.20	0.63	...	0	z	
412032.....	8 43 25.58	45 02 34.6	20.35	0.01	0.90	0.17	...	0	z	
402599.....	8 43 23.48	44 35 48.6	20.39	-0.20	1.05	0.07	...	0	z	
406753.....	8 42 10.45	44 47 25.9	20.41	-0.21	1.29	0.31	...	0	z	
408501.....	8 42 27.43	44 52 40.2	20.41	-0.04	1.17	0.26	...	0	z	
408890.....	8 40 28.34	44 53 16.9	20.44	-0.35	1.40	0.60	...	0	q, t	
409279.....	8 41 48.12	44 54 40.8	20.47	-0.06	0.96	0.15	...	0	z	
406391.....	8 41 48.87	44 46 12.7	20.48	-0.06	0.95	0.35	0.1464	3	z	
407199.....	8 40 20.29	44 48 22.6	20.49	-0.22	0.95	0.08	...	0	B, z	
405761.....	8 41 19.31	44 44 28.5	20.49	0.10	0.68	0.09	...	0	t	
405709.....	8 41 54.55	44 44 27.9	20.49	-0.08	0.99	0.21	...	0	z	
404114.....	8 43 18.14	44 40 12.2	20.50	-0.48	0.93	0.49	0.5910	4	A, A	
400119.....	8 43 23.93	44 28 49.4	20.50	-0.26	1.05	0.46	0.2631	1	z	
400182.....	8 42 02.35	44 28 46.2	20.50	-0.02	0.88	0.00	...	0	z	
410133.....	8 42 41.88	44 57 14.2	20.52	-0.05	0.90	0.02	...	0	z	
403390.....	8 41 32.20	44 37 47.5	20.52	0.12	0.89	0.09	...	0	t	
409345.....	8 41 58.41	44 54 54.9	20.55	-0.05	1.13	0.24	...	0	t	
409425.....	8 42 21.84	44 55 15.3	20.58	0.11	0.81	0.42	...	0	z	
408068.....	8 41 34.53	44 51 16.0	20.58	0.14	0.90	-0.08	...	0	z	
406249.....	8 42 06.66	44 45 53.4	20.58	-0.03	0.96	0.45	0.1775	2	z	
402214.....	8 40 45.43	44 34 09.2	20.59	0.01	1.05	0.64	...	0	z	
405871.....	8 43 12.07	44 45 05.3	20.65	-0.08	0.96	0.44	0.9868	1	z	
401067.....	8 42 47.49	44 31 26.4	20.65	-0.70	0.28	0.11	2.1625	6	z	
408431.....	8 43 26.12	44 52 38.4	20.71	-0.32	1.55	0.50	...	0	F	
410483.....	8 43 09.65	44 58 13.8	20.77	0.04	0.87	0.14	...	0	z	
409986.....	8 41 20.82	44 56 32.2	20.81	-0.05	0.72	0.13	...	0	z	
403888.....	8 42 58.20	44 39 28.7	20.90	-0.16	0.68	0.54	0.1329	5	A, A	
400263.....	8 42 46.38	44 29 09.4	21.13	-0.50	0.28	0.21	...	0	z	
411356.....	8 40 23.36	45 00 06.7	21.14	-0.45	1.13	0.39	...	0	E	
403862.....	8 43 16.29	44 39 27.1	21.26	...	1.60	0.66	0.4854	5	A	
404878.....	8 42 18.19	44 42 13.3	21.38	-0.42	0.74	-1.57	...	0	t	
403235.....	8 43 06.36	44 37 42.4	21.39	-0.60	0.55	0	t	
411892.....	8 41 52.72	45 01 52.5	21.45	-0.14	1.41	0.47	...	0	v	
411145.....	8 41 53.97	44 59 50.9	21.46	-0.01	1.17	1.11	0.3140	5	v	
408592.....	8 43 21.61	44 53 06.6	21.53	-0.95	2.12	0.37	...	0	F	
411772.....	8 42 00.90	45 01 37.2	21.65	-0.08	0.96	1.02	...	0	v	
411555.....	8 41 58.10	45 01 04.5	21.69	-0.68	1.19	0.61	...	0	v	
411444.....	8 41 50.66	45 00 43.1	21.93	-0.50	0.88	0.35	...	0	v	

Col. (1).—Identifying serial number.

Col. (2).—Right ascension in hours, minutes, and seconds (1950 equinox).

Col. (3).—Declination in degrees, arcminutes, and arcseconds (1950 equinox).

Col. (4).—Total R_F magnitude. In SA 57 and SA 68, this means the magnitude within a circular aperture of radius $2r_1$. In Herc 1 and Lynx 2, this means the FOCAS total magnitude (magnitude within an area at least twice the size of that contained within the detection isophote).

Cols. (5), (6), (7).—In SA 57 and SA 68, the colors are derived from magnitudes measured in a circular aperture of radius $2r_1$. In Herc 1 and Lynx 2, the colors are derived from magnitudes measured in a circular aperture of radius $2''$.

Col. (8).—Redshift. Objects with a redshift of 0.0000 were morphologically classified as galaxies, but spectroscopically found to be stars.

Col. (9).—Redshift quality: $q = \min [6, \min (1, N_{\text{def}}) + 2N_{\text{def}} + N_{\text{prob}}]$, where N_{def} and N_{prob} are the number of definite and probable features, respectively.

Col. (10).—Sources of the redshift: (A—OO) multihole or multislit spectrum from the specified mask (cross-reference to col. [1] in Table 5); (a—z) long-slit or multifiber spectrum from the specified observing run (cross-reference to col. [1] in Table 3); (1) H. Spinrad, 1980, private communication; (2) E. L. Turner, 1980, private communication; (3) based on observations obtained at the W. M. Keck Observatory, which is operated jointly by the California Institute of Technology and the University of California.

Col. (11).—Number of galaxies, brighter than this galaxy in R_F and within the field of view of this galaxy's primary mask, for which no spectra were ever obtained and no other redshifts exist.

Col. (12).—Number of galaxies, brighter than this galaxy in R_F and part of the statistical sample defined by this galaxy's primary mask, that have been observed spectroscopically but lack definite redshifts ($q > 2$). If this value is -1 , then all galaxies brighter than this galaxy in R_F that are within the field of view of this galaxy's primary mask have $q > 2$ redshifts.

NOTES.—(B) Special target of the mask, selected as a bright galaxy; (C) special target of the mask, selected as a member of a cluster of galaxies; (J) special target of the mask, selected as a member of a faint B_J -selected sample; (N) special target of the mask, selected as a candidate narrow emission line galaxy (NELG); (R) special target of the mask, selected as a radio source; (U) special target of the mask, selected as a UV-excess source; (X) not targeted by the mask, but accidentally fell within a slitlet or slit targeted at a different object.

TABLE 7
 PHOTOMETRIC ERROR

Band (m_0)	SA 57	SA 68	Herc 1	Lynx 2
U (23)	0.70	0.43	0.33	0.27
B_j (24)	0.37	0.51	0.34	0.46
R_F (23)	0.35	0.56	0.50	0.46
I_N (21)	0.97	0.41	0.27	0.21

NOTE.—Values of Gaussian σ expressed as fraction of flux at reference magnitudes (m_0) for each band in each field.

letter indicates that the object was observed either with a long slit or a multifiber setup during the run associated with that letter (cross-reference with col. [1] in Table 3). A numeral indicates a source external to the survey, as listed in the table notes. If the first source in the list of redshift sources of column (10) is a multiaperture mask, then the object potentially belongs to that mask's statistical sample. Column (13) indicates whether the object is a special target within that sample. An "X" indicates that the object was

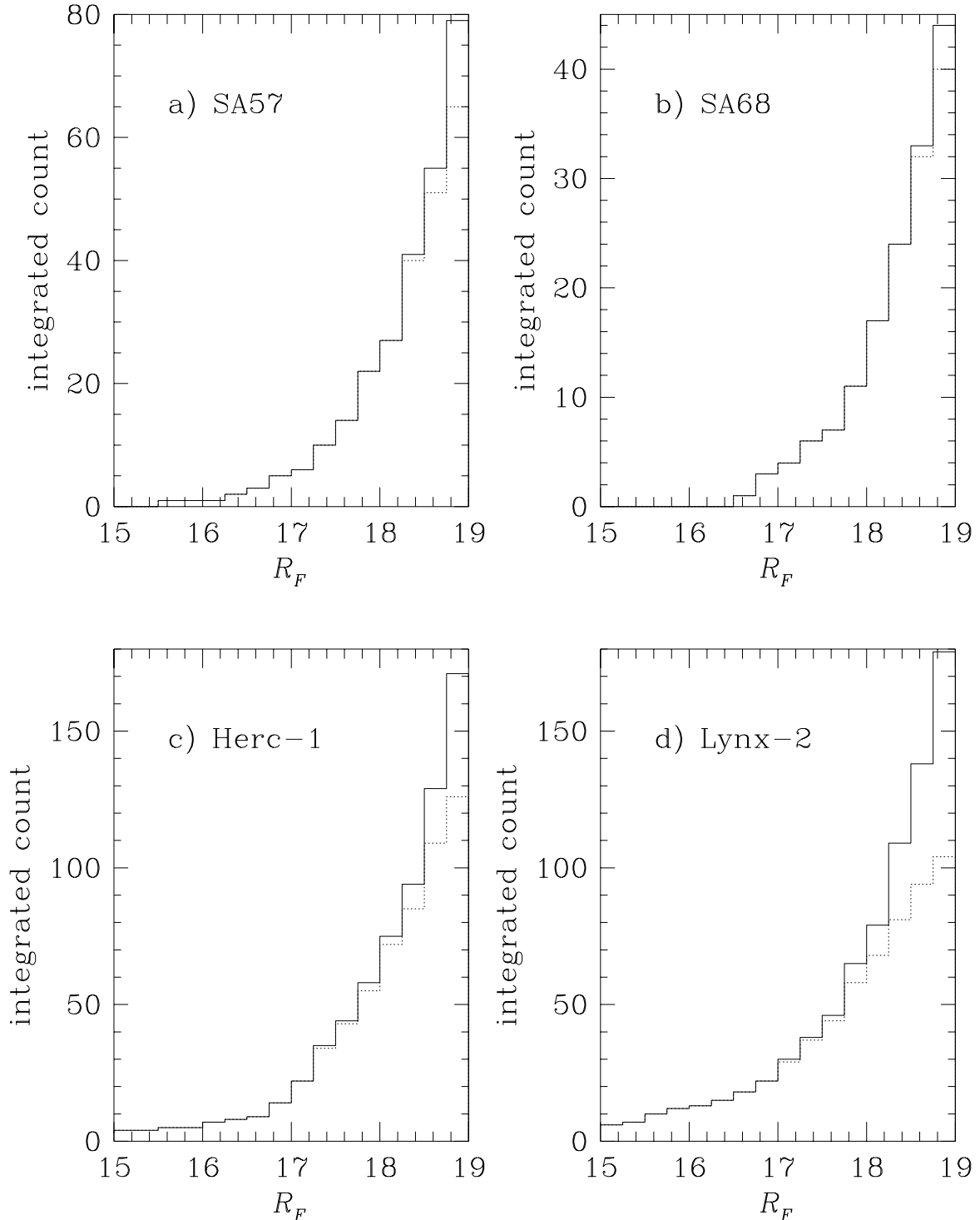


FIG. 1.—Integrated counts vs. R_F for the bright R_F -limited samples. The solid lines are for the complete photometric galaxy samples. The dotted lines are for those galaxies with acceptable redshifts ($q > 2$).

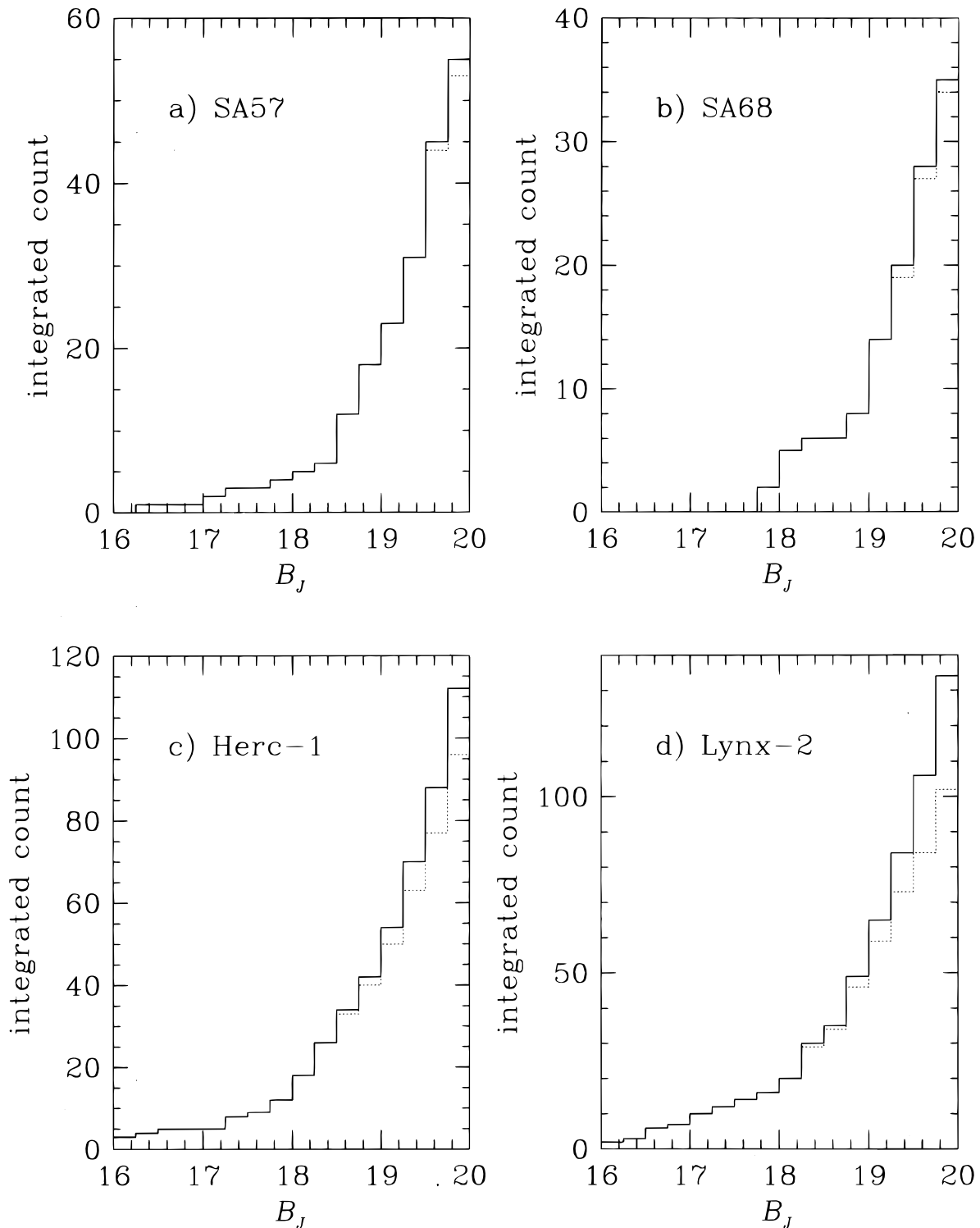


FIG. 2.—Integrated counts vs. B_J for the bright B_J -limited samples. The solid lines are for the complete photometric galaxy samples. The dotted lines are for those galaxies with acceptable redshifts ($q > 2$).

not targeted by the mask but that a spectrum was obtained as its light accidentally fell down one of the slitlets. Any other letter indicates that the object is a special target of the mask and therefore should be excluded from that mask's statistical sample, unless the sample is complete to that object's R_F magnitude. If there is no code listed, the object belongs to that mask's statistical sample. For objects within a mask's statistical sample and with a reliable redshift ($q > 2$), column (11) gives the number of galaxies within the

field of view of the mask, and brighter in R_F than the object, for which no spectra of any quality were ever obtained and no external sources of a redshift exist (N_b). Column (12) lists, for objects within a mask's statistical sample and with a reliable redshift, the number of galaxies within that mask's statistical sample, and brighter in R_F than the object, for which a spectrum was attempted but no reliable redshift was obtained (N_b). If this number is -1 , then all galaxies within the field of view of the mask, regardless of whether

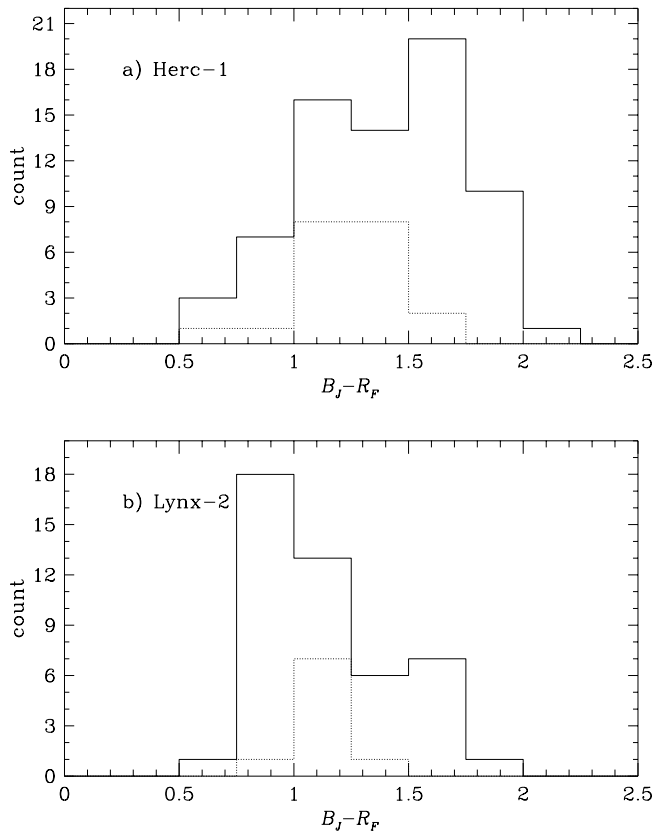


FIG. 3.—Distribution in $B_J - R_F$ of those objects in Herc 1 and Lynx 2 in the magnitude range $18 < R_F \leq 19$ that have been observed spectroscopically, split into those with (solid lines) and without (dotted lines) acceptable redshifts ($q > 2$).

they belong to the statistical sample or not, and brighter in R_F than the object, have reliable redshifts.

The “faint statistical sample” is the subset of objects within the survey statistical sample with $R_F > 19$. This division is made here purely for presentational purposes, to avoid overlap with the bright R_F -limited sample. Figure 4 shows the distribution in R_F of the faint statistical samples in SA 57, SA 68, and Herc 1 (Lynx 2 is not part of the faint survey). The entire sample over all three fields, fainter than $R_F = 19$, contains 448 extended objects, of which acceptable redshifts ($q > 2$) have been obtained for 259. Four of these were found spectroscopically to be misclassified stars. The distribution of the remaining 255 reliable galaxy redshifts has a median redshift of 0.291. Of those 255 galaxies, 188 have $N_b = 0$ or $N_b = -1$ (i.e., acceptable redshifts have been obtained for all brighter objects in the statistical sample of its mask) and thus constitute the least biased (though certainly not bias-free) subsample of the faint survey. Three objects in the faint statistical sample have $B_J \leq 20$ and thus are also part of the bright B_J -limited survey; all three have acceptable redshifts.

4.5. Additional Faint Galaxies

In addition to the bright R_F -limited and B_J -limited samples and the faint statistical samples, a large number of other extended objects have been observed spectroscopically as part of other programs. Most are parts of well-defined statistical samples, in particular, a survey of faint blue extended objects (Smetanka 1997) and a survey of faint radio sources (Kron, Koo, & Windhorst 1985). Some

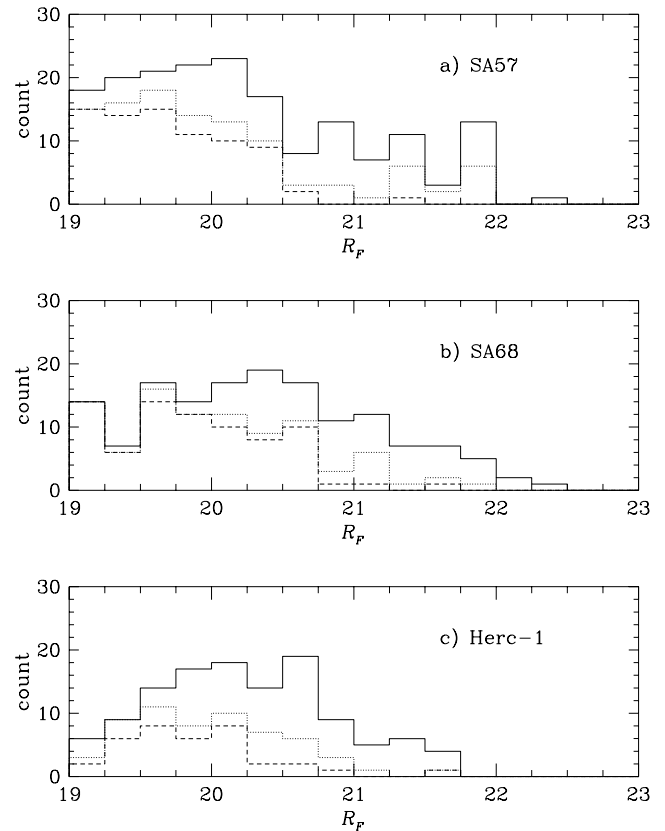


FIG. 4.—Distribution in R_F of the faint statistical samples. The solid lines are the observed samples. The dotted lines are those with acceptable redshifts ($q > 2$). The dashed lines are those with acceptable redshifts and either $N_b = 0$ or $N_b = -1$ (i.e., acceptable redshifts have been obtained for all brighter objects in the statistical sample of its mask).

objects were targeted because they were individually interesting. Included in this group of objects are special targets of the multiaperture masks that did not make it into the statistical samples. While the selection functions for these samples are not described here, the individual objects are included in the catalogs, as the redshifts were obtained during the same spectroscopic observing runs. Combined over all four fields, an additional 403 extended objects were observed spectroscopically, of which 156 have reliable ($q > 2$) redshifts. Six of these are misclassified stars.

5. SUMMARY

This paper presents in an integrated fashion the data for our main pencil-beam photometric and spectroscopic surveys conducted over the last 15 years. The survey is distinguished by the excellence of its photometry in four separate passbands ($UB_J R_F I_N$), as well as by the depth of the survey. We have achieved good completeness over the whole of the four fields to limits of roughly $R_F < 19$ and $B_J < 20$ (the “bright sample”), largely the result of wide-field fiber spectroscopy. Within three of these main fields, we have probed ~ 2 mag deeper in many separate $5'$ subfields with a multislit spectrograph. These subfields are characterized by the galaxies within them, by which of these galaxies we targeted spectroscopically, and by which of the latter we obtained reliable redshifts for. In addition to this faint “statistical sample” and the “bright sample,” we also report redshift measurements for a substantial number of faint galaxies whose selection was in some way biased.

The redshift survey is summarized in Figure 5, which plots the logarithm of the redshift versus R_F for galaxies with reliable redshifts in each of the four fields separately, with different symbols used to represent each galaxy's membership in the statistical samples. The most notable feature of these plots is the initial result discussed in § 1: the clustering of the redshifts in each field within a few redshift “spikes.”

Many of these data have been used in a preliminary form in previous papers (e.g., Koo & Kron 1988; Broadhurst et al. 1990). Subsequent papers will apply these data to the analysis of the large-scale spatial distribution of galaxies, the luminosity function of galaxies, the evolution of faint galaxies, and the calibration of photometric redshift determinations.

We would like to thank the directors and many staff at KPNO who have made this large program possible in terms

of both hardware and software support over the duration of this project; special thanks are extended to J. DeVeny, P. Massey, S. Barden, B. Schoening, F. Valdes, and J. Barnes. We are also grateful for the help of R. Harrington of the US Naval Observatory in providing astrometric support; of H. Marshall, who provided vital computing support for the reductions of many of the data; of the DEEP Team and Keck Observatory in providing additional observing time; and of R. Guzman, who assisted with reductions of the Keck data. We also want to acknowledge the support by several of our colleagues during various observing runs, including R. Windhorst, A. Szalay, and N. Ellman. This work was supported by NSF grants AST 81-21653, AST 83-14232, AST 87-05517, AST 88-14251, AST 88-58203, AST 91-20005, and AST 90-21378; NASA graduate fellowship NGT 50677 (M. A. B.); NASA Hubble Fellowships HF-1028.01-92A (M. A. B.) and HF-1036.01-92A (S. R. M.), from the Space Telescope Science Institute, which is oper-

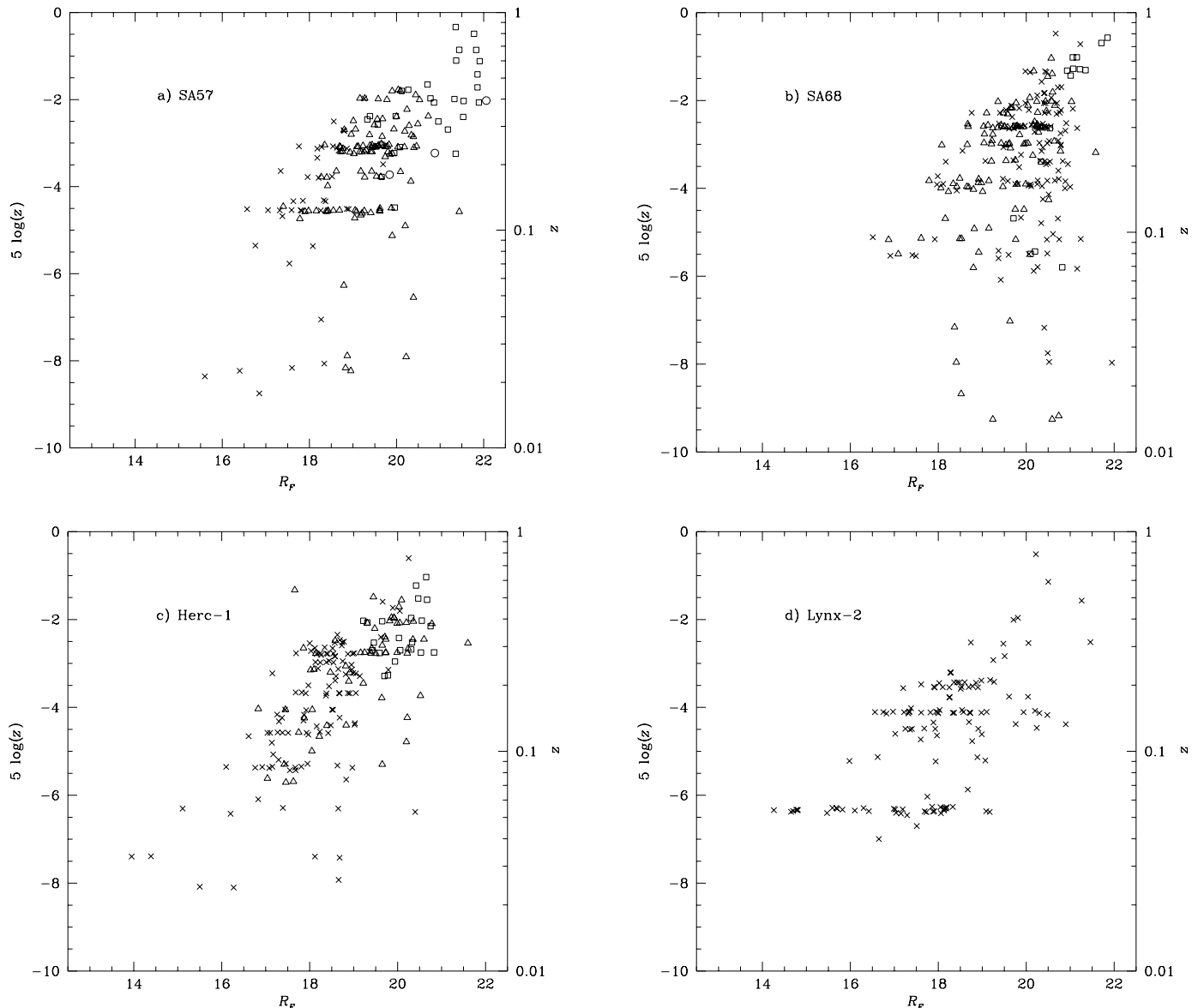


FIG. 5.—Logarithm of the redshift vs. R_F for all galaxies with acceptable redshifts ($q > 2$) in each of the four fields. Different symbols are used to represent an object's inclusion in the statistical samples: *triangles*, included in the statistical sample, with either $N_b = 0$ or $N_b = -1$; *squares*, included in the statistical sample, with $N_b > 0$; *circles*, not part of the statistical sample, but was a special target of a multiaperture mask; *crosses*, not part of the statistical sample. Objects 308890 ($5 \log z = -12.614$, $R_F = 12.58$) and 307977 ($5 \log z = -12.343$, $R_F = 16.88$) are beyond the lower edge of the plot for Herc 1.

ated by the Association of Universities for Research in Astronomy, Inc., under contract NAS 5-26555; the Space Telescope Science Institute's Associate Program (J. A. M.); and US-Hungarian Science and Technology Grant J. F. No. 010/90 (D. C. K.). D. C. K. would like to acknowledge

the Department of Terrestrial Magnetism of the Carnegie Institution of Washington and the Space Telescope Science Institute for their financial support of this program while he was a postdoctoral fellow.

REFERENCES

- Barden, S. C., Armandroff, T., Massey, P., Groves, L., Rudeen, A. C., Vaughn, D., & Muller, G. 1993, in ASP Conf. Proc. 37, *Fiber Optics in Astronomy II*, ed. P. M. Gray (San Francisco: ASP), 185
- Barden, S. C., & Massey, P. 1988, in ASP Conf. Proc. 3, *Fiber Optics in Astronomy*, ed. S. C. Barden (San Francisco: ASP), 140
- Baum, W. 1962, in IAU Symp. 15, *Problems of Extra-Galactic Research*, ed. G. C. McVittie (New York: Macmillan), 390
- Bershady, M. A., Hereld, M., Kron, R. G., Koo, D. C., Munn, J. A., & Majewski, S. R. 1994, *AJ*, 108, 870 (Paper III)
- Broadhurst, T. J., Ellis, R. S., Koo, D. C., & Szalay, A. S. 1990, *Nature*, 343, 726
- Broadhurst, T. J., Ellis, R. S., & Shanks, T. 1988, *MNRAS*, 235, 827
- Bruzual A., G., & Kron, R. G. 1980, *ApJ*, 241, 25
- Butcher, H. 1982, *Proc. SPIE*, 331, 296
- Colless, M., Ellis, R. S., Taylor, K., & Hook, R. N. 1990, *MNRAS*, 244, 408
- Cowie, L. L., Songaila, A., & Hu, E. M. 1991, *Nature*, 354, 460
- Glazebrook, K., Ellis, R., Colless, M., Broadhurst, T., Allington-Smith, J., & Tanvir, N. 1995, *MNRAS*, 273, 157
- Jarvis, J. F., & Tyson, J. A. 1981, *AJ*, 86, 476
- Kirshner, R. P., Oemler, A., & Schechter, P. 1978, *AJ*, 83, 1549
- Kirshner, R. P., Oemler, A., Schechter, P., & Shectman, S. 1981, *ApJ*, 248, L57
- Koo, D. C. 1981, Ph.D. thesis, Univ. California, Berkeley
- . 1985, *AJ*, 90, 418
- . 1986, *ApJ*, 311, 651 (Paper II)
- Koo, D. C., & Kron, R. G. 1987, in IAU Symp. 124, *Observational Cosmology*, ed. A. Hewitt, G. R. Burbidge, & L.-Z. Fang (Dordrecht: Reidel), 383
- . 1988, in *Towards Understanding Galaxies at Large Redshifts*, ed. R. G. Kron & A. Renzini (Dordrecht: Kluwer), 209
- Koo, D. C., Kron, R. G., & Szalay, A. S. 1987, in 13th Texas Symposium on Relativistic Astrophysics, ed. M. P. Ulmer (Singapore: World Sci.), 284
- Kron, R. G. 1980, *ApJS*, 43, 305 (Paper I)
- Kron, R. G., Koo, D. C., & Windhorst, R. A. 1985, *A&A*, 146, 38
- Lilly, S. J., Le Fèvre, O., Crampton, D., Hammer, F., & Tresse, L. 1995, *ApJ*, 455, 50
- Loh, E. D., & Spillar, E. J. 1986, *ApJ*, 303, 154
- Majewski, S. R. 1992, *ApJS*, 78, 87
- Majewski, S. R., Aldering, G. S., Kron, R. G., & Koo, D. C. 1997, in preparation
- Majewski, S. R., Kron, R. G., Koo, D. C., & Bershady, M. A. 1994, *PASP*, 106, 1258
- Smetanka, J. 1997, *MNRAS*, submitted
- Songaila, A., Cowie, L. L., Hu, E. M., & Gardner, J. P. 1994, *ApJS*, 94, 461
- Tinsley, B. M. 1980, *ApJ*, 241, 41
- Tonry, J., & Davis, M. 1979, *AJ*, 84, 1511
- Turner, E. L. 1980, in IAU Symp. 92, *Objects of High Redshift*, ed. G. O. Abell & P. J. E. Peebles (Dordrecht: Reidel), 71
- Valdes, F. 1982, *Proc. SPIE*, 331, 465
- . 1986, *Proc. SPIE*, 627, 749